2021

CONTRIBUTION OF MATERNAL mRNA PROVISIONING TO EMBRYONIC STRESS RESPONSE IN A REEF-BUILDING CORAL

Erin Elizabeth Chille
University of Rhode Island, erin_chille@uri.edu

CONTRIBUTION OF MATERNAL mRNA PROVISIONING TO EMBRYONIC STRESS RESPONSE IN A REEF-BUILDING CORAL

BY

ERIN ELIZABETH CHILLE

A THESIS SUBMITTED IN PARTIAL FULFILLMENT OF THE

REQUIREMENTS FOR THE DEGREE OF

MASTER OF SCIENCE

IN

BIOLOGICAL AND ENVIRONMENTAL SCIENCE

UNIVERSITY OF RHODE ISLAND

2021

MASTER OF SCIENCE

OF

ERIN ELIZABETH CHILLE

APPROVED:

Thesis Committee:

Major Professor Hollie Putnam

Steven Irvine

Ying Zhang

Brenton DeBoef
DEAN OF THE GRADUATE SCHOOL

UNIVERSITY OF RHODE ISLAND
2021

ABSTRACT

Prior to fertilization, mothers provision their oocytes with mRNA that regulates the early stages of development and may additionally include transcripts for proteins that support embryonic stress response early on. At some point during embryogenesis, however, these maternal transcripts are degraded as zygotic transcription activates and intensifies during a phenomenon known as the maternal-to-zygotic transition (MZT). Some evidence suggests that as the MZT progresses, and the effects of maternal transcripts are waning while the zygotic expression is being established, offspring of marine broadcast spawners become more vulnerable to environmental perturbations. In light of escalating threats to marine broadcast spawners, it is critical to understand their reproduction and development, which are essential processes for species resilience by repopulating and replenishing existing populations. Reef building corals, in particular, are under threat from multiple stressors at the local and global scales. Mass mortality has occurred in recent years due to a series of marine heatwaves. In addition, there is chronic stress occurring in the form of ocean acidification, or the decline in pH in surface waters due to the uptake of atmospheric carbon dioxide of anthropogenic origin. Here, we characterize the function of maternal mRNAs, the timeline of the MZT, and sensitivity of gene expression to ocean acidification (OA) in the reef- building coral, *Montipora capitata* to investigate role of the MZT in embryonic stress response in reef-building corals.

In Manuscript 1, we examine gene expression over nine developmental stages in *Montipora capitata* from eggs and embryos at 1, 4, 9, 14, 22, and 36 hours-post-fertilization (hpf), as well as swimming larvae (9d), and adult colonies. Weighted

Gene Coexpression Network Analysis revealed four expression peaks, identifying the maternal complement, two waves of the MZT, and adult expression. Gene ontology enrichment revealed maternal mRNAs are dominated by cell division, methylation, biosynthesis, metabolism, and protein/RNA processing and transport functions. The first MZT wave occurs from ~4-14 hpf and is enriched in terms related to biosynthesis, methylation, cell division, and transcription. In contrast, functional enrichment in the second MZT wave, or ZGA, from 22 hpf-9dpf, includes ion/peptide transport and cell signaling. Finally, adult expression is enriched for functions related to signaling, metabolism, and ion/peptide transport. Our proposed MZT timing is further supported by expression of enzymes involved in zygotic transcriptional repression (Kaiso) and activation (Sox2), which peak at 14 hpf and 22 hpf, respectively. Further, DNA methylation writing (DNMT3a) and removing enzymes (TET1) peak and remain stable past ~4 hpf, indicating that methylome programming occurs before 4 hpf.

In Manuscript 2, we quantify gene expression sensitivity to ocean acidification across a set of developmental stages in *Montipora capitata*. Developing embryos were exposed to three pH treatments ranging from 7.8 (Ambient), 7.6 (Low) and 7.3 (Xlow) from fertilization to 9 days post-fertilization. Embryo and planula volume and gene expression were compared between treatments at each developmental stage to determine the effects of acidified seawater on early development. While there was no measurable size differentiation between fertilized eggs and the prawn chip stage (9 hpf) exposed to ambient, low, and extreme low pH, early gastrula and planula raised in low and extreme low pH treatments were significantly smaller than those raised in

ambient seawater, suggesting an energetic cost to developing under low pH. However, no differentially expressed genes emerged between treatments at any time point, except swimming larvae (9 dpf). In a global analysis, principal components analysis shows stronger variation due to life stage, with PC1 showing separation of the life stages and representing 83% of the variance in expression. This suggests that either ocean acidification is not very stressful to organisms not actively calcifying, or that the maternal-to-zygotic transition is robust to pH stress. Planula, however, showed a strong response to reduced pH. Notably, larvae developing at pH 7.8 (Ambient) and pH 7.3 (Xlow) were more similar than those developing at pH 7.6 (Low), which may be due to high CO_2 stimulation of symbiont function at pH 7.3. There was not enough expression data available from the symbiont to test this hypothesis here. Larvae from pH 7.6 showed upregulation of genes involved in cell division, regulation of transcription, lipid metabolism, and oxidative stress in comparison to the other two treatments, supported by smallest sizes in this treatment. While low pH appears to increase energetic demands and trigger oxidative stress, the developmental process is robust to this at a molecular level.

Our high-resolution insight into the coral maternal mRNA and MZT provides essential information regarding setting the stage for, and the sensitivity of, developmental success and parental carryover effects under increasing environmental stress. Additionally, identifying the genes, pathways, and functions underlying the response capacity of embryonic and larval corals to future conditions such as ocean acidification is critical to forecasting coral population resistance and resilience to disturbance.

ACKNOWLEDGMENTS

I would like to express my deepest appreciation for my advisor, Dr. Hollie Putnam, who was my best academic cheerleader, coach, advocate, and guide. I would also like to express my deepest gratitude to my incredible lab members, Maggie Schedl, Kevin Wong, Emma Strand, Sam Gurr, Dennis Conetta, Danielle Becker, Jill Ashey, Hannah Reich and Ariana Huffmyer. Thank you for all your advice, laboratory, field support, and writing support, and for being the best Zoom work buddies. I would also like to thank to my thesis committee members, Dr. Steven Irvine, and Dr. Ying Zhang for your encouragement and constructive criticism. For assistance with running bioinformatic analyses, I would like to thank Erin Roberts, Dr. Jon Puritz, and Kevin Bryan. I would like to thank Dr. Graham Forrester for your guidance, encouragement, and profound belief in my in my abilities from the start of my academic career at the University of Rhode Island. Finally, I would like to thank my amazing family, partner, and friends, whose unwavering support and love helped make this project possible.

PREFACE

This thesis has been prepared in Manuscript Format. Manuscript 1, entitled "Developmental series of gene expression clarifies maternal mRNA provisioning and maternal-to-zygotic transition in the reef-building coral *Montipora capitata*", has been prepared for submission to *Genome Biology*, and currently is available as a preprint on bioRxiv. Manuscript 2, entitled "Development in corals with vertically-transmitted symbionts is resistant to ocean acidification", is currently in preparation for submission to *Proceedings of the Royal Society B.* Additional authors for each manuscript are listed at the beginning of each chapter. Appendices are presented at the end of the thesis and contain the supplementary material for each manuscript.

TABLE OF CONTENTS

LIST OF TABLES

TABLE PAGE

Chapter 1:

TABLE PAGE

LIST OF FIGURES

FIGURE PAGE

Chapter 1:

MANUSCRIPT 1

Prepared for submission to *Genome Biology*.

Developmental series of gene expression clarifies maternal mRNA provisioning and maternal-to-zygotic transition in the reef-building coral *Montipora capitata*

Chille E[1*], Strand E[1], Neder M[2,3], Schmidt V[4], Sherman M[1], Mass T[2], Putnam HM[1]

Affiliations
[1] Department of Biology, University of Rhode Island, Rhode Island, USA
[2] Department of Marine Biology, The Leon H. Charney School of Marine Sciences, University of Haifa, Haifa, Israel
[3]The Interuniversity Institute of Marine Science, 88103 Eilat, Israel
[4] Yale School of Medicine, Yale University, Connecticut, USA

***Corresponding author:** echille124@gmail.com

Abstract

Background

Maternal mRNA provisioning of oocytes regulates early embryogenesis. Maternal transcripts are degraded as zygotic genome activation (ZGA) intensifies, a phenomenon known as the maternal-to-zygotic transition (MZT). Here, we examine gene expression over nine developmental stages in the Pacific rice coral, *Montipora capitata*, from eggs and embryos at 1, 4, 9, 14, 22, and 36 hours-post-fertilization (hpf), as well as swimming larvae (9d), and adult colonies.

Results

Weighted Gene Coexpression Network Analysis revealed four expression peaks, identifying the maternal complement, two waves of the MZT, and adult expression. Gene ontology enrichment revealed maternal mRNAs are dominated by cell division, methylation, biosynthesis, metabolism, and protein/RNA processing and transport functions. The first MZT wave occurs from ~4-14 hpf and is enriched in terms related to biosynthesis, methylation, cell division, and transcription. In contrast, functional enrichment in the second MZT wave, or ZGA, from 22 hpf-9dpf, includes ion/peptide transport and cell signaling. Finally, adult expression is enriched for functions related to signaling, metabolism, and ion/peptide transport. Our proposed MZT timing is further supported by expression of enzymes involved in zygotic transcriptional repression (Kaiso) and activation (Sox2), which peak at 14 hpf and 22 hpf, respectively. Further, DNA methylation writing (DNMT3a) and removing enzymes

(TET1) peak and remain stable past ~4 hpf, indicating that methylome programming occurs before 4 hpf.

Conclusions

Our high-resolution insight into the coral maternal mRNA and MZT provides essential information regarding setting the stage for, and the sensitivity of, developmental success and parental carryover effects under increasing environmental stress.

Keywords: time course, WGCNA, epigenetics, resilience, oocyte, embryo

Background

Under escalating threats from anthropogenic climate change, coral reefs are experiencing massive population declines globally [1]. Contributing to the global destabilization of coral reef ecosystems is the decreased fitness of coral during its early development [2–5] due to anthropogenic climate change [6–8]. The majority of corals (~85%) are broadcast spawners [9], releasing eggs and sperm into the water column where fertilization and embryogenesis occur [10]. Over the course of hours to days, embryos develop into planula larvae [10] and may spend several hours to weeks in the water column, or searching the benthos for an appropriate location to settle and metamorphose into coral spat [11]. This prolonged pelagic period constitutes an ontogenetic bottleneck for corals and other broadcast-spawning marine organisms, during which they are particularly sensitive to the climate-related stressors [6,7].

Acute temperature stress can be lethal to coral embryos and larvae, while ocean acidification can have sub-lethal effects [7], including decreased fertilization efficiency [12,13] and metabolic depression [14–17]. Other conditions co-occurring with climate change, including high and low salinity, hypoxia, and exposure to UV radiation, can also decrease fitness during development [7,8]. The cumulative effects of these unprecedented stressors on early development may compromise recruitment, the process in which offspring repopulate and replenish declining populations, further contributing to the destabilization of coral reef ecosystems [2].

Several studies on the sensitivity of embryonic development have shown that the earliest life stages are robust to climate-related stressors, but embryos become more vulnerable as gastrula and planula [6,7,18–22]. This has generally been attributed to the loss of maternal defenses, such as heat shock proteins, during the course of development [6,7,18–22]. During oogenesis, maternally-derived mRNAs (or parentally-derived in the case of hermaphroditic species), along with other gene products (i.e. transcription factors, cofactors), are loaded into eggs [23,24]. As gametes and early embryos do not yet contain the molecular machinery necessary to regulate gene expression, these mRNAs direct early development until the zygotic molecular machinery is able to take over [23]. The maternal mRNA complement is the result of selection in response to life history [24,25], and can be primed to support embryonic resilience to predictable stressors [26–28]. For example, it has been shown that in cichlids, the maternal mRNA complement differs by trophic specialization [25]. Additionally, many organisms can prime the immune response of their offspring by providing increased levels of mRNAs coding for immune response-related enzymes [25,27–31]. In terms of marine invertebrates, the annelid *Hediste diversicolor*, was found to store higher levels of the antimicrobial peptide hedistin in the oocytes after an immune challenge [28], and sea urchins with different life history strategies (lecithotrophy or planktotrophy) were found to differentially provision oocytes with mRNAs related to oxidative stress [32].

Maternal provisioning may explain the resilience of early coral embryos to expected stressors, and is a mechanism of coral reef resilience that is only starting to be fully

investigated [33–36]. However, there is growing concern that maternal provisioning may not provide adequate defense against rapid climate change, especially for organisms living at the edge of their physiological limits [7,22,24,37]. For example, coral bleaching from temperature stress can negatively impact maternal provisioning of protein, lipid, mycosporine-like amino acids and carotenoids in the eggs [38]. Consequently, characterization of the coral maternal mRNA complement can additionally provide essential information regarding setting the stage for, and the sensitivity of, developmental success under increasing environmental stressors.

While maternal provisioning may protect the embryo from expected stressors early on, these gene products only persist for a limited time, after which point embryo vulnerability appears to intensify [6,7,18–22]. In a process known as the maternal-to-zygotic transition (MZT), maternal gene products are degraded as zygotic transcription activates and intensifies [39–41]. The loss of maternal defenses during this process has been posited to contribute to higher morbidity and mortality in fish gastrula, sea urchin blastula/gastrula, as well as many marine invertebrate larvae during exposure to environmental stressors [7,20–22,37].

The MZT and many of the molecular mechanisms underlying its regulation are conserved in metazoans [39,40,42–44]. Maternal mRNA clearance is mediated both maternally, primarily by the enzyme Smaug [45,46], and zygotically [40]. Transcriptional repressors, including the maternally-derived enzyme Kaiso [47,48], prevent zygotic transcription until a stable, open chromatin state is achieved [49].

Once this occurs, ZGA begins gradually and ramps in intensity as it progresses [39,40]. The low-intensity beginning of ZGA (the “first” or “minor” wave) is controlled by maternal transcription factors, including Sox2 [50], while the ramping of ZGA to higher intensities (the “major wave”) is triggered by the clearance of the majority of maternal transcripts and the lengthening of the cell cycle through the degradation of cell-cycle regulators such as Cyclin-B [39,51]. Among the first of the enzymes shown to be zygotically expressed in sea urchins and other organisms are those involved in bauplan formation, including Wnt8 and Brachyury (TBXT) [52–54]. Upon culmination of the MZT, zygotically-derived gene products regulate developmental progression and homeostasis [39]. Characterizing the timeline of the MZT in reef-building corals in regards to these conserved mechanisms will help to establish the time period during which maternal defenses are active, and at which point coral embryos may become more susceptible to environmental perturbations.

Enzymes linked to epigenetic modification are also shown to be key players in the repression and activation of zygotic transcription, with increases in DNA methylation and simultaneous decreases in chromatin accessibility associated with the onset of ZGA [40,55]. Additionally, these enzymes confer potential mechanisms for cross-generational plasticity, which may additionally buffer reef-building corals and other organisms from the effects of unprecedented stressors [56,57]. Several key epigenetic modification associated enzymes that provide transcriptional regulation capacity include: DNA methyl-transferases (DNMT3a, DNMT1), the histone deacetylase recruiting enzyme ubiquitin-like containing PHD and RING finger domains 1

(UHRF1), and methyl-binding domains (MBD2, MBD3), as well as the active demethylation enzyme ten-eleven translocation enzyme (TET1) and chromatin regulation enzyme brahma-related gene-1 (BRG1). DNMTs are responsible for laying down DNA methylation *de novo* (DNMT3a) and maintaining DNA methylation through mitosis (DNMT1) [58], while TET1 actively removes DNA methylation [59]. Depletion of DNMT1 can lead to the premature onset of ZGA in *Xenopus* embryos [60]. The protein UHRF1 is associated with DNMT1, marking hemimethylated DNA for DNMT1 activity [61]. The closely-related MBD2 and MBD3 proteins are also involved in transcriptional repression as components of the Mi-2/NuRD corepressor complex [62–64]. In mice, it has been suggested that MBD3 is essential for embryo viability as a key component of the Mi-2/NuRD corepressor complex, while MBD2 may be a functionally redundant cofactor [64]. Finally, BRG1 proteins are derived from the maternal mRNA complement and are suggested to be the first gene required for ZGA in mammals [65]. BRG1 is generally associated with increasing chromatin accessibility because of its role in breaking the bonds between DNA and histones through ATP hydrolysis. Analyzing the expression profiles of these specific enzymes involved in epigenetic modification may provide further support on the epigenetic state necessary for ZGA.

Here we used the knowledge on the well-documented spawning of the Pacific rice coral *Montipora capitata* in Hawai‘i [66,67] and its physical development [68] to examine developmental timing through the lens of gene expression. In this study, we examine gene expression dynamics across nine life stages from pre-fertilization to

adult, focusing on shifts in the gene expression network within the first 24 hours post-spawning. In doing so, we aim to characterize the *M. capitata* maternal mRNA complement, as well as the timing and functional patterns of ZGA and the MZT. This high-resolution analysis of the *M. capitata* developmental transcriptome will provide a basis from which to investigate how its early developmental stages respond to environmental stressors, as well as the potential for carryover or latent effects due to parental history.

Results

RNA sequencing, quality control, and mapping

TruSeq Illumina Stranded Paired-End (PE) sequencing of cDNA libraries prepared following polyA enrichment resulted in 935,000,000 PE reads with an average of 19,392,156 reads per sample. After quality filtering and adapter removal, 694,800,000 PE reads remained with an average of 14,241,176 reads per sample. The average alignment rate was 79.28 ± 1.945384% mean ± sem. The GFFcompare results showed that a total of 63,227 genes queried from the mapped GTF files were matched to the 63,227 genes in the reference genome [69]. Altogether, there were 40,883 matching intron chains, 63,218 matching loci, and zero missing elements.

Global gene expression patterns

Pre-filtering to retain genes with counts over 10 in at least 8.3% of samples (i.e., the proportion representing a single life stage) resulted in 32,772 genes for statistical analysis. A principal components analysis conducted with this gene set shows

significant differences in global gene expression between time points with the exception of samples corresponding to unfertilized and fertilized eggs, which cluster together. Differences in gene expression between life stages is primarily explained by PC1 and PC2, which account for 71% and 14% of variation in expression, respectively (Fig 2). WGCNA assigned genes into 34 modules, with 48 to 11,142 genes in each module, one of which, module Grey, contains 29 genes that did not fit with any other group. Modules exhibited nine distinct expression profiles (Fig 3 left axis) based on module clustering by eigengene dissimilarity. Further, clustering of life stages by module-trait correlation identified four expression groups, which we call developmental clusters throughout this manuscript (Fig 3, clustering on top axis). The first developmental cluster, the "Maternal" modules, contains unfertilized and fertilized eggs (modules grey, coral1, lightslateblue, mediumpurple3, antiquewhite2, antiquewhite4, thistle, honeydew1, and midnightblue). The second developmental cluster, the "ZGA Wave 1" modules, contains the life stages cleavage, prawn chip, and early gastrula (modules magenta4, indianred3, blue2, plum3, blue4, skyblue1, brown2, coral, darkslateblue, plum4, and violet). The third developmental cluster, the "ZGA Wave 2" modules, contains the life stages mid-gastrula, late gastrula, and planula (modules magenta4, skyblue1, darkseagreen, darkslateblue, thistle4, salmon4, mediumpurple1, sienna3, salmon, and blue). Finally, the fourth developmental cluster, "Adult", contains only the adult samples (modules antiquewhite4, thistle, navajowhite1, blue, cyan, blueviolet, and ivory).

Functional annotation

To provide up-to-date gene ontology (GO) annotation for functional enrichment analysis, functional annotation was undertaken using DIAMOND, InterProScan, Blast2GO, and Uniprot [70–73]. Sequence alignment using DIAMOND resulted in 55,217 significant pairwise alignments for the total 63,227 sequences queried, with a median e-value of 3.100000e-72 and a median bitscore of 282.3. Blast2GO mapped 4,205 sequences to one or more GO terms. Additionally, a UniProt search of the protein identifiers obtained through DIAMOND matched 2,351 sequences with one or more GO terms (7,408 total terms). Finally, annotation with InterProScan matched 49,338 out of the 63,227 query sequences to entries in the InterProScan databases, 20,603 of which were associated with one or more GO terms (47,726 total terms). In total, 3,264 unique GO terms were mapped to 23,107 genes, with a total of 55,974 annotations to the *M. capitata* transcriptome (Table S1).

Functional Enrichment

Functional enrichment analysis was undertaken for each life stage (Table S1) and for the four developmental clusters: Maternal, ZGA Wave 1, ZGA Wave 2, and Adult (Fig. 4, Fig. 5). The maternal complement has 92 enriched biological processes (Table S3) primarily related to cell division, DNA repair, methylation, biosynthesis, metabolism, and protein/RNA processing and transport and 92 enriched molecular functions (Table S3) primarily related to binding, translation, transmembrane transport, and enzymatic activity. The first wave of the ZGA is enriched in 55 biological process terms (Table S4) and 60 molecular function terms (Table S4).

Biosynthesis activity remains high during the first wave of the ZGA, which is additionally associated with enrichment of GO terms related to RNA processing and histone assembly. The second wave of the ZGA is enriched in 22 biological process terms (Table S5) of transmembrane transport and DNA metabolic process, as well as 47 molecular function terms, corresponding to transport, oxidation-reduction process, and binding. Finally, the adult transcriptome is enriched in 31 biological process terms (Table S6) and 54 molecular functions. GO terms related to metabolism and transmembrane transport remain high in the adult transcriptome, in addition to terms related to cell signaling.

Expression of Developmental Biomarkers

The expression profiles of six developmental biomarker genes involved in the MZT and later development were assessed to test if our WGCNA-based timeline of the MZT was supported by these key developmental players. Several orthologs of MZT biomarkers were found using BLAST, including Cyclin-B (7 hits), Smaug (3 hits), Kaiso (90 hits), Sox2 (18 hits), Wnt8 (23 hits), and TBXT (15 hits). The expression profiles of these six genes, all of which showed significantly different expression patterns across life stages (Table S4A), indicate their specific temporal activity during early development (Fig 6). Firstly, Cyclin-B is highly expressed in unfertilized eggs up until cleavage. However, after this point its expression decreases monotonically until the planula stage (Fig. 6i). Next, both Smaug and Kaiso experience significant upregulation after fertilization and downregulation after the prawn chip stage (Fig. 6ii-iii). Then, during the early gastrula stage the zygotic transcription activator, Sox2,

significantly peaks after which point it is rapidly downregulated (Fig. 6iv). Wnt8 appears to be lowly expressed in early on and is downregulated further after cleavage. However, it later significantly peaks in expression between the early gastrula and planula stages of development (Fig. 6v). Finally, TBXT is significantly upregulated starting after cleavage, leading to an expression peak that lasts until after the planula stage (Fig. 6vi).

Expression of Epigenetic Biomarkers

Targeted expression analysis of seven epigenetic biomarkers was also conducted to elucidate the epigenetic landscape necessary for the MZT. A Blast search of the *M. capitata* transcriptome reported 3 DNMT3a hits, 4 DNMT1 hits, 1 TET1 hit, 2 MBD2 hits, 1 MBD3 hit (shared with MBD2), 2 UHRF1 hits, and 84 BRG1 hits. The top hits of these seven genes all showed significantly different expression patterns across life stages (Table S7). Temporal expression of these epigenetic enzymes revealed three distinct patterns in expression (Fig 7). First, for all seven enzymes, expression levels changed very little between the samples representing unfertilized eggs and fertilized eggs. After fertilization, DNMT1, MBD2/3, and UHRF1 decrease in expression throughout development (Fig. 7ii, 7iv, 7v). For DNMT1, while expression appears to decrease overall throughout development, a small peak in expression occurs during late gastrulation. For MBD2/3, expression appears to plateau after the initial decrease following fertilization, while expression of UHRF1 appears to decrease monotonically throughout development (Fig. 7iv, 7v). In contrast to DNMT1, MBD2/3, and UHRF1, the expression of DNMT3A, TET1 and BRG1 increases significantly after fertilization and later plateaus. For TET1 and DNMT3A transcription appears to

stabilize after cleavage, however BRG1 continues to be significantly upregulated until the prawn chip stage before plateauing.

Discussion

In this study, developmental gene expression of the reef-building coral, *Montipora capitata* was examined to characterize the maternal mRNA complement and function in oocytes and the timeline of the maternal to zygotic transition (MZT). In sampling nine time points, with six time points occurring within thirty-six hours of fertilization, our dataset provides the highest temporal resolution to date that captures complex gene expression dynamics underlying the MZT. WGCNA facilitated the identification of the maternal mRNA complement, two waves of ZGA, and adult expression. These results, along with targeted expression analysis of six developmental biomarkers provides evidence that the MZT begins before cleavage (4 hpf) and continues through gastrulation. The expression profiles of seven epigenetic enzymes provide further support for the timing of the MZT and the epigenetic state necessary for ZGA in *M. capitata*. These findings provide an essential framework for future research on mechanisms of resilience in early developmental stages and the potential for parental carryover effects under increasing environmental stressors.

Maternal Provisioning

The active maternal mRNA complement, here defined as the modules significantly positively correlated with either the unfertilized and fertilized egg samples, was enriched in biological processes primarily related to housekeeping functions (e.g.

vacuolar transport [GO:0007034], spliceosomal snRNP assembly [GO:0000387], D-amino acid metabolic process [GO:0046416], and DNA replication [GO:0006260]). This is unsurprising as the primary function of maternal mRNA provisioning is to regulate early development until the molecular machinery of the zygote is able to take over [23]. Extensive work across animal phyla shows enrichment of housekeeping functions in eggs [26,74–76]. For example, in a study comparing the maternal mRNA complement of *Lymnaea stagnalis* with maternal transcriptomes across the animal kingdom, it was found that the 5-10% of maternal mRNAs conserved across phyla consisted primarily of functions such as nucleotide binding, protein degradation and activities associated with the cell cycle [26]. Indeed, in our analysis via WGCNA, we found support for significantly enriched GO terms (Table S3.) commonly associated with cell cycle, biosynthesis, transcription, signaling, and protein processing functions. This reinforces results from a prior GO analysis via enrichment of genes expressed in both female and male gametes with 100TPM threshold from these same three unfertilized egg samples [33].

High representation of mRNAs involved in DNA damage repair in the maternal complement (e.g., DNA damage checkpoint [GO:0000077], DNA repair [GO:0006281], recombinational repair [GO:0000725], interstrand cross-link repair [GO:0036297], cellular response to ionizing radiation [GO:0071479], and positive regulation of apoptotic process [GO:0043065]) likely prevents the proliferation of damaged cells during the rapid cell cycles occurring during the first few hours of development. Embryonic development is particularly sensitive to DNA damage, as the

accumulation of damaged cells can quickly lead to embryonic death [77–79]. Embryos of broadcast spawning species, especially those of vertically transmitters that pass down symbionts in the eggs [80], are particularly at risk of DNA damage due to exposure to ultraviolet (UV) radiation [81–84]. UV radiation can damage DNA both indirectly, through the production of reactive oxygen species that can lead to the oxidation of nucleotides, and directly by dimerization of neighboring pyrimidines [85–87]. Prolonged exposure to UV-radiation during early development may necessitate maternal frontloading of DNA repair mechanisms in broadcast spawners [81–84]. For example, one study showed that anchovy eggs spawned under light and dark conditions have an innate capacity for UVB-induced DNA repair, but that diel cycles of DNA repair mechanisms (likely zygotically-derived) did not occur until approximately six hours post-fertilization [84]. In another case, Antarctic meroplankton species that spawn during the Austral summer have been shown to have a higher capacity for DNA damage repair than species that spawn during the winter [83]. As a tropical broadcast spawning species with vertical transmission of symbionts [67,88], *Montipora capitata* embryos are particularly susceptible to DNA damage incurred from UV radiation and from ROS production by their endosymbionts [80,89–91], which may partially explain the enrichment of DNA repair functions in the *M. capitata* maternally-provisioned oocyte transcriptome.

While the gene expression time course analyzed here provides insight into the maternal complement, we acknowledge that our analysis may not be comprehensive. The expression of maternal mRNAs in the embryo is primarily regulated through the

modulation of the poly-A tail [23,39,41,92,93], with elongation of the poly-A tail leading to transcriptional activation and shortening of the poly-A tail leading to de-activation [23,39,41,92,93]. As our sequence library preparation (polyA enrichment) primarily excludes un-adenylated mRNAs, it is likely that some un-adenylated transcripts, potentially related to stress-response functions in the maternal mRNA complement, were not fully captured in these libraries. Absolute determination of maternal mRNAs (adenylated and un-adenylated) in the oocytes could be better served via ribosomal RNA depletion library preparation prior to sequencing, as suggested in [40].

MZT Timeline

With the exception of non-parthenogenetic insects, in most metazoans, fertilization triggers egg activation and is associated with the elimination of approximately 30% of maternal transcripts [39,49,94,95]. The clearance of these maternal mRNAs marks the first event of the MZT [39,49]. In *M. capitata*, a wave of maternal transcript degradation, marking the beginning of the MZT, appears to be starting by 1-4 cell divisions (4 hpf). As sampling time increases beyond 1 hpf, the maternal complement (modules grey, coral1, lightslateblue, mediumpurple3, antiquewhite2, antiquewhite4, thistle, honeydew1, and midnightblue) shows a substantial reduction of correlation of eigengene expression with life stage (Fig. 3), supporting the downregulation of transcripts that are associated with unfertilized and fertilized eggs. This is further evidenced by the significant downregulation of maternally-provisioned Cyclin-B mRNAs starting by 4 hpf (Fig. 6i), and a peak in the expression of Smaug (Fig. 6ii)

between cleavage (4 hpf) and prawn chip (9 hpf), signaling the de-adenylation of maternal transcripts during this period. After the clearance of maternal mRNAs between fertilization and cleavage, the clustering of life stages by module eigengene correlation (Fig. 3) supports two temporal peaks in expression, suggesting that in *M. capitata*, the MZT progresses in two waves. The first wave appears to occur between 4 and 14 hpf, as indicated by the clustering of eigengene-lifestage correlations of cleavage, prawn chip, and early gastrula samples, while the clustering of mid-gastrula, late gastrula, and planula samples support a second wave occurring between 22hpf and 9dpf. While we hypothesize the ZGA is ongoing until settlement, as indicated by the unique expression pattern in the adult transcriptome, the transfer of developmental control to the zygote, marking the conclusion of the MZT, likely occurs much earlier. However, the discrimination of transcripts as "maternal" or "zygotic" in origin can be complicated because the activation of existing mRNAs by polyadenylation cannot be distinguished from the activation of newly-transcribed mRNAs, as discussed above. As such, we cannot distinguish the absolute end of the MZT, which is marked by the transition of developmental control from maternal to zygotic molecular machinery [39]. In the future, the termination of the MZT could be more fully captured through the characterization of Single Nucleotide Polymorphisms (SNPs) in the maternal and paternal transcriptomes, as described in [96], zygotically-derived transcripts can be identified by the presence of paternal SNPs. For corals, this would best be accomplished through making crosses between eggs and sperm from known parental colonies.

Taken in concert, the expression profiles of key developmental enzymes provide a temporal progression illustrating the molecular mechanisms underlying zygotic genome activation in *M. capitata*. Peaks in the expression of Cyclin-B, Smaug, Kaiso, and Sox2 (Fig 3i-3iv) indicate that maternal mRNA clearance and ZGA during the first wave of the MZT in *M. capitata* is mediated by maternal mRNAs. Indeed, the polyadenylation of maternal mRNAs after fertilization have been implicated in both maternal mRNA degradation [45,46,51] and ZGA [50,53,97] in bilaterians. The expression profiles of these enzymes during *M. capitata* and sea anemone (*Nematostella vectensis*) MZT [98] supports that maternal regulation of the first MZT wave is a conserved feature from basal metazoan development. Further, the peak in maternal transcriptional regulator Kaiso in the prawn chip samples (9 hpf), followed by the peak in maternal transcription factor Sox2 in the early gastrula samples (14 hpf) suggests that ZGA is repressed until early gastrulation in *M. capitata*. This is further supported by a substantial increase in the correlation of eigengene expression with time during and after the early gastrula stage in module clusters 5, 8, and 9 (Fig. 3 Y axis), and a gradual shift in dominance of the enrichment of RNA and protein processing-related biological processes in the cleavage stage (Table S2C) to terms related to transcription in the early gastrula stage (Table S2E).

Several factors including nucleocytoplasmic ratio, chromatin accessibility, cell cycle destabilization, and maternal mRNA degradation have been implicated in the initiation of zygotic transcription [39]. In *N. vectensis*, yeast, and the African clawed frog cell cycle destabilization appears to facilitate the activation of zygotic

transcription [98–101]. In *Nematostella vectensis*, this is shown by a decrease in Cyclin-B between 2 and 7 hpf followed by ZGA between 7 and 12 hpf. In *M. capitata*, Cyclin-B also decreases after cleavage (4 hpf), showing cell cycle destabilization. While cell cycle destabilization likely plays a role in ZGA in *M. capitata*, increasing chromatin accessibility (see "Epigenetic state for ZGA") and the weakening of maternal transcriptional repression through the de-adenylation of maternal mRNAs, indicated by a peak in RNA binding protein Smaug between 4 and 9 hpf, likely also contribute to ZGA.

While the first wave of the MZT appears to be regulated through maternal mRNAs, a shift in positive eigengene correlations from modules in cluster 4 to modules in clusters 8 and 9 between early and mid-gastrulation (Fig 3) shows the upregulation of genes that were either previously lowly expressed, or completely unexpressed between 14 and 22 hpf. A significant decrease in the expression of Sox2 during this transition indicates that zygotic, rather than maternal, transcription factors may be implicated, supporting the identification of this temporal peak in gene expression as the second wave of ZGA. While expression of Wnt8 and TBXT peaks during this second wave is expected due to their roles in bauplan specification during gastrulation [98,102,103], their continual upregulation despite the downregulation of Sox2 suggests that they may be zygotically transcribed in *M. capitata*, as shown in *Xenopus* and in sea urchins. [53,54,97]. Besides bauplan specification, similarly to [98] ion/peptide transport and cell signaling-related processes are upregulated during the second wave (Fig 4C). Interestingly, we also see upregulation of GO terms related to response to

environmental stress (i.e. xenobiotic transport (GO:0042908) and response to oxidative stress (GO:0006979)), as well as terms related to symbiosis (i.e. reduction of food intake in response to dietary excess (GO:0002023), response to glucose (GO:0009749), multicellular organism growth (GO:0035264), glycerolipid biosynthetic process (GO:0045017), carbohydrate biosynthetic process (GO:0016051) and glycolipid biosynthetic process (GO:0009247)), in the late gastrula (Table S2G) and planula stages (Table S2H), suggesting that by late gastrulation (36 hpf) *M. capitata* embryos are able to sense the environment and tune transcription in response to environmental stimuli. The combined loss of maternal defenses at the start of the MZT and low homeostatic capacity has been suggested to contribute to embryo vulnerability in fish, sea urchins, and other marine broadcast spawners [6,7,18–22]. As such, the period ranging from the start of maternal mRNA clearance (≤4 hpf) to transcriptional plasticity in response to stimuli (≤36 hpf) may represent the most sensitive stages and thus present a critical bottleneck in *M. capitata* early development.

While the timing and scale of maternal transcript degradation and ZGA during the MZT is shown to vary between species [40], the timing of MZT described here is remarkably similar to other anthozoans with similar developmental courses. For example, gene expression time courses during *Acropora digitifera [34]*, *Acropora millepora [35]*, and *Nematostella vectensis [98]* development suggest the onset of ZGA occurs within the first 24 hours of development. In *A. digitifera*, clustering of the expression patterns in early life stages mirrored the clustering of life stages here [34].

In *A. digitifera*, the prawn chip (9 hpf) and early gastrula (14 hpf) stages grouped together, and late gastrula (48 hpf), planula (96 hpf), and adult stages grouped together [34]. Likewise, a shift in gene expression between cleavage (4 hpf) and gastrulation (22 hpf) in *A. millepora* supports the onset of ZGA during the early gastrula stage [35]. The sea anemone, *N. vectensis*, also shows similar gene expression dynamics during the MZT to *M. capitata*, with maternal degradation in *N. vectensis*, potentially occurring between cleavage (2 hpf) and prawn chip (7 hpf), and ZGA beginning by the onset of gastrulation (12 hpf; [98]. While the genera *Acropora* and *Montipora* belong to the same family of reef-building corals (Acroporidae), *N. vectensis* belongs to different sub-class in the anthozoan lineage. However, the four species are all broadcast spawning anthozoans with similar developmental timelines and embryonic courses (i.e. form a prawn chip; [34,68,104,105], suggesting that the timing of the MZT, and potentially the molecular mechanisms underlying MZT regulation, may be evolutionarily conserved within cnidarians. If so, this would have important implications for research on carryover effects and transgenerational plasticity, which depends heavily on the rapid accumulation of knowledge surrounding gene expression regulation and epigenetic state during reef-building coral development [56,106]. Much of this knowledge has already been generated in the model cnidarian, *N. vectensis* [98,107], and may provide a strong baseline for such studies.

Epigenetic state for ZGA

Epigenetic programming during the MZT has a key role in the repression and activation of zygotic transcription [40,55], and additionally presents a potential

mechanism for heritable, non-genetic phenotypic plasticity allowing for the rapid acclimatization of reef-building corals to rapid environmental change [56,106]. However, epigenetic programming during the MZT has primarily been described in mammals and non-mammalian vertebrates and likely differs greatly from epigenetic programming during the development of reef-building corals and other invertebrates [108–111]. In mammals, parental epigenetic marks are erased twice during the MZT, and are replaced with marks that are necessary for embryo viability [112,113], making epigenetic inheritance rare in mammals [108]. However, nonmammalian vertebrates appear to inherit the paternal methylome, reprogramming the maternal methylome to match before ZGA begins [114]. Epigenetic programming during the MZT is only starting to be understood in invertebrates, as historic invertebrate models (e.g., *Drosophila melanogaster and Caenorhabditis elegans*) lack cytosine DNA methylation almost entirely [114], and the invertebrate species studies thus far appear to lack epigenetic reprogramming entirely (e.g., sponges, honey bees, ctenophores, sea urchins, and sea squirts; [108,109,111,115]. Indeed, a recent work on reef-building corals shows that epigenetic marks may be transferred between generations, and suggests that the paternal and maternal methylomes appear to contribute equally to the methylome of the offspring [110].

Generally, in vertebrates and mammals in particular, chromatin structure is relatively open prior to ZGA, and decreases in accessibility during the MZT as DNA methylation increases [40,116,117]. While chromatin structure condenses over time, local DNA accessibility remains open during ZGA to facilitate the activation of

specific genes [40,116,117]. However, this appears to not be the case for invertebrates. For example, the bivalves *Crassostrea gigas* and *Patinopecten yessoensis*, are shown to have heavy methylation in the oocytes, which peaks during the blastula/gastrula stage before declining and remaining at stable levels for the remainder of development [118,119]. In other invertebrates, such as honey bees and sponges, DNA methylation levels tend to be stable throughout early development [109,111,115]. While methylation levels were not measured here, significant changes in the expression enzymes linked to methylation activity may hint to the epigenetic landscape necessary for ZGA in *M. capitata*.

The expression patterns of key the epigenetic regulators assessed here provide the first data characterizing the dynamics of genes involved in epigenetic programming underlying the MZT in *M. capitata* and further sets the stage for future research on the mechanisms of epigenetic inheritance in reef-building corals. Here, significant changes in the expression of six out of seven of these genes between the samples representing fertilized eggs (1 hpf) and cleaving embryos (4 hpf) correlates with the start of the MZT. DNMT3a and TET1 responsible for de novo methylation and methylation removal, respectively, are two of these six enzymes that change between 1to 4 hpf and then maintain stable expression for the remainder of development, suggesting that the embryo methylome programming occurs during this short window. Completion of methylome programming may be necessary for the start of the MZT, as it has been shown in zebrafish that harmonization of the paternal and maternal methylomes is necessary for the successful progression of ZGA [120]. A sharp

decrease in transcriptional repression through MBD2/3 by the cleavage stage may signal the completion of methylome harmonization. Accordingly, research on the mechanisms underlying the transfer of epigenetic marks from parent to offspring and harmonization of the embryonic methylome in reef-building corals may benefit from frequent sampling and quantification of methylation between fertilization (0 hpf) and cleavage (4 hpf).

Several mechanisms of epigenetic modification appear to set the stage for ZGA after embryonic methylome programming in *M. capitata*. Firstly, passive (de)-methylation is likely to be the primary regulator of DNA methylation during the MZT due to rapid cell division. While expression of DNMT3a (*de novo* methylation) and TET1 (methylation removal) stabilizes after cleavage, DNMT1 (methylation maintenance) shows significant expression fluctuations during the MZT. After initial down-regulation of DNMT1 prior to cleavage, methylation maintenance activity appears to remain stable through the first wave of the MZT. However, it is significantly downregulated again at the start of the second wave of the MZT (during mid-gastrulation), prior to returning to previous expression levels. This depression of methylation maintenance provides support to the hypothesis that increasing local chromatin accessibility facilitates the activation of specific loci [40,118,121]. Increasing local chromatin accessibility is further evidenced by upregulation of BRG1 from pre-cleavage (1 hpf) until the prawn chip stage (9 hpf), which may additionally facilitate the start ZGA during early gastrulation. Other mechanisms of epigenetic modification with putative roles in the MZT [49], including histone arginine and

lysine methylation (GO:0034969, GO:0034968), histone acetylation (GO:0016573), and protein ADP-ribosylation (GO:0006471) were enriched in the maternal complement (Table S2) and during the first wave of ZGA (Table S3), supporting multiple conserved mechanisms of epigenetic regulation of the MZT between model organisms and *M. capitata*.

Conclusions

As anthropogenic climate change continues to alter the marine environment at an accelerating and unprecedented rate, it is more important than ever to understand the mechanisms underlying the resilience and sensitivity of vulnerable ontogenetic stages. Future research evaluating potential avenues of rapid acclimatization in reef-building corals, including parental effects, carryover effects, and cross-generational plasticity, relies on the generation of baseline knowledge on parental molecular provisioning, the epigenetic landscape during early development, and temporal gene expression dynamics during the MZT [56]. Here, our characterization of maternal mRNA provisioning and the maternal-to-zygotic transition in *Montipora capitata* sets the stage for these future studies and additionally identifies cleavage (≤4 hpf) through late gastrulation (≤36 hpf) as a potential critical window during *Montipora capitata* development.

Methods

Study System

Endemic to the Hawaiian archipelago, *Montipora capitata* is a dominant and ecologically important inhabitant of lagoons and fringing reefs [67,122–124]. Studies have shown that *M. capitata* is more tolerant to environmental stressors compared to other reef-building corals due to its perforate skeleton and deep tissues [125,126]. However, the earliest life stages of this species may be more susceptible to climate change-related and local anthropogenic stressors than adults. Like many other marine invertebrates, *M. capitata* has a complex early life history. It is a hermaphroditic broadcast spawner with vertical symbiont transmission [67,88]. The early life history of *Montipora spp.*, from fertilization through larval body formation, has been well-documented by Okubo and others [68].

Specimen collection

M. capitata egg-sperm bundles were collected (Hawai‘i Department of Land & Natural Resources Special Activity Permit 2018-50) from the reef adjacent to the Hawai‘i Institute of Marine Biology (HIMB) Kāne‘ohe Bay, Hawai‘i (21°25'58.0"N 157°47'24.9"W) during their release on June 13, 2018. *M. capitata* adult fragments were collected from the reef adjacent to HIMB and Reef 11.13 (1°27'07.7"N 157°47'40.3"W) and acclimated in ambient conditions (27 °C, ~480 µatm) mesocosm tanks for two weeks prior to snap freezing on September 22nd, 2018.

Experimental set-up

Immediately after collection, 300 uL of egg and sperm bundles were snap frozen and stored at -80 °C while the rest of the bundles were placed in conical chambers to break apart and hydrate for 10 minutes. 300 uL of eggs were separated from the sperm and rinsed 3 times with 0.2 uM filtered seawater then snap-frozen and stored at -80 °C. Fertilization and early development (0 h - ~16 hfp) took place in 3 replicated 1.6L flow through conical chambers and further development (~ 16 hpf - 9 d) took place in small (6 x 6 cm) flow through bins within larger 74L flow through tanks, both under ambient temperature ~26.8°C. Water flow to each conical was controlled with ½ GPH Pressure Compensating Drippers and held at a maximum potential flow rate of 7.57 liters per hour. For a 1.6 L conical, the turnover rate was once every ~50 minutes and for a 74L tank, the turnover rate was once every ~ 23 hours. The average light intensity of the experimental setup was measured using a handheld PAR sensor (Underwater Quantum Flux Apogee instruments - Model MQ-510; accuracy = ±4%) and was 115.8 ± 14.7 µmol m^{-2} s^{-1}, n=6 measurements. Temperature, salinity, and pH were measured three times daily using a handheld digital thermometer (Fisherbrand Traceable Platinum Ultra-Accurate Digital Thermometer, accuracy = ±0.05 °C, resolution = 0.001°) and a portable multiparameter meter (Thermo Scientific Orion Star A-series A325; accuracy = ±0.2 mV, 0.5% of PSU reading, resolution = 0.1 mV, 0.01 PSU) with pH and conductivity probes (Mettler Toledo InLab Expert Pro pH probe #51343101; Orion DuraProbe 4-Electrode Conductivity Cell Model 013010MD), respectively. Temperature and pH probes were calibrated using Tris (Dickson Laboratory Tris Batch 27, Bottles 70, 75, 167, 245, and 277) standard

calibrations. Throughout the experiment, the temperature, salinity, and pH of tanks and conicals (mean±SEM) was 26.99±0.075°C, 34.24±0.017 psu, and -52.84±0.348 mV, respectively.

Sample collection and preservation

Samples were collected at nine time points. Sampling times (Fig. 1) represent visually-distinct developmental stages including unfertilized eggs (immediately after bundle breakup; n=3) and multiple stages at various hours post fertilization (hpf), fertilized egg (1 hpf; n=2), cleavage (4 hpf; n=3), prawn chip (9 hpf; n=3), early gastrula (14 hpfg; n=3), mid-gastrula (22 hpf; n=2), late gastrula (1.5 days post fertilization; n=2), and planula (9 days post fertilization; n=3). Molecular samples, 300 µL/replicate of gametes, embryos, and larvae, or whole adult fragments (~5x7 cm; n=3), were snap-frozen in liquid nitrogen and stored at -80°C until RNA extraction.

RNA extraction, sequencing, and read processing

Developmental samples were digested at 55°C in 300 µL DNA/RNA Shield for two to three-and-a-half hours and centrifuged at 2200 rcf for one minute to separate the remaining solids. A small clipping of each adult sample was vortexed in 2 mL 0.5 mm glass bead tubes (Fisher Scientific Catalog No. 15-340-152) with 1 mL of DNA/RNA Shield for two minutes at high speed. Total RNA was extracted from each supernatant with the Zymo Quick-DNA/RNA™ Miniprep Plus Kit (Zymo Research, Irvine, CA, USA) following the manufacturer's protocol for tissue samples. RNA was quantified

with a ThermoFisher Qubit Fluorometer and quality was measured with an Agilent TapeStation 4200 System. Total RNA samples were then sent to Genewiz (South Plainfield, New Jersey, USA) for library preparation and sequencing. cDNA libraries were constructed following the TruSeq Stranded mRNA Sample Preparation Protocol (Illumina) using polyA enrichment and were sequenced on a HiSeq instrument at Genewiz targeting 15 million reads per sample.

Read quality was assessed with FastQC (v0.11.8) and compiled with MultiQC [127,128]. Following quality assessment, reads were trimmed to remove adapters and low-quality reads using FastP [129]. Sequences were filtered for quality applying a five base pair sliding window to remove reads with an average quality score of 20 or less. The sequences retained had quality scores greater than or equal to 20 in at least 90% of bases and a sequence length greater than or equal to 100 bases. Read quality was re-assessed with FastQC (v0.11.8) and then aligned and assembled using HISAT2 in the stranded paired-end mode [130] in combination with StringTie in the stranded setting (v2.1; [131]. Following assembly, mapped GFFs were merged for assessment of precision and accuracy and compared to the *M. capitata* reference assembly GFF using GFFcompare (v0.11.5; [132]. A gene count matrix was then generated from the GFFs using the StringTie *prepDE* python script [131].

Global gene expression analysis

All gene expression analyses were performed in RStudio (v1.3.959), using R version 4.0.2 [133]. First, genes with low overall expression were filtered using Genefilter's (v1.70.0) *pOverA* filter function [134]. Given that the smallest number of replicates

was two, genes with fewer than 10 counts in at least 2 out of 24 samples (*pOverA* 0.083, 10) were excluded from further analysis. Counts were then normalized with DESeq2's (v1.28.1) variance stabilizing transformation (vst; [135] after confirming that all size factors were less than 4. To visualize experiment-wide patterns in gene expression, a principal coordinates analysis (PCA) based on sample-to-sample distances was performed on the vst-transformed gene counts using the DESeq2 *plotPCA* function (Fig. 2).

Transformed counts were used for a Weighted Gene Co-expression Network Analysis (WGCNA; [136]. WGCNA analysis is a data reduction approach that assigns genes with similar expression patterns to co-expression groups called modules. Using this technique allowed us to identify groups of genes with similar expression profiles across developmental time. All samples were used for WGCNA after visually checking for outliers in an unrooted hierarchical tree built with the R stats *hclust* "average" function [133]. In order to construct a topological overlap matrix similarity network to assess gene expression adjacency, the WGCNA *pickSoftThreshold* function was used to explore soft threshold values from 1 through 30. A soft thresholding power of 23 (scale-free topology fit index of 0.85) was chosen and used to construct a topological overlap matrix similarity network using signed adjacency. Modules were identified from this topological overlap matrix similarity network using the WGCNA package *dynamicTreeCut* function with the settings deepSplit 2, and minimum module size 30. Modules with greater than 85% eigengene similarity were

merged and the resulting finalized 34 modules were used for expression plotting, module-trait correlation, and gene ontology enrichment analysis.

Clustering of WGCNA expression modules by eigengene dissimilarity using the *hclust* "average" method identified 9 clusters of modules. Expression profile plots were generated for each cluster by plotting the mean eigengene expression value of each of the replicate samples per time point for each module (Fig. S1). Additionally, module-trait correlation was assessed by calculating gene significance (the correlation between the gene and the time point) and module membership (the correlation of the module eigengene and the gene expression profile; [136]. Correlation values were plotted as a heatmap using the *complexHeatmap* package [137]. Modules with a p-value less than or equal to 0.05 were considered significantly correlated with a timepoint (Fig. 3). Finally, the distinct expression phases in the MZT were identified by clustering life stages by their module-trait correlation using the *hclust* "average" method to build an unrooted hierarchical tree.

Gene ontology mapping and enrichment analysis

Comprehensive gene ontology (GO) annotation of the reference genome was undertaken for subsequent functional enrichment analysis using InterProScan (v.5.46-81.0), Blast2GO (v5.2), and UniProt [71–73]. First, homologous protein sequences were identified using the DIAMOND (v2.0.0) *blastx* program in "more sensitive" mode to map predicted cDNA sequences against the NCBI non-redundant (nr) protein database (downloaded on August 6, 2020) using an e-value cut-off of 1e-05 and a

block size of 20 [70]. Concurrently, InterProScan's *iprlookup* function was run to map GO terms from the InterPro database (accessed on August 24, 2020) to the *M. capitata* predicted protein sequences [69,71]. Next, the XML output files from DIAMOND and InterProScan were both loaded into Blast2GO for compilation and further mapping using the obo database (updated August 11, 2020; [72]). Additional GO terms were extracted from the UniProtKB database by searching for protein identifiers obtained via DIAMOND using UniProt's "Retrieve/ID mapping tool" [73]. Finally, mapping results from Blast2GO and UniProt were compiled in RStudio (v1.3.959), using R (v-4.0.2; [133]).

Gene ontology enrichment analysis was performed to characterize the functions provided by the maternal mRNA complement and the changes in the embryo's functional toolkit during the MZT. Modules that were significantly correlated ($p<0.05$) with the maternal and adult complements and each phase of the MZT, as well as each life stage, were identified. The genes comprising each module within a group of interest were compiled and subsetted from the counts matrix for functional enrichment analysis. The R package *Goseq* (v1.40.0) was used to perform GO term enrichment analysis, therefore taking gene length bias into account [138] when determining the functional profiles of each group. Subsequently, the R package *simplifyEnrichment* (v0.99.4) was used to visualize the enriched biological process and molecular function terms for each group [139]. With this package, a semantic similarity matrix for a set of GO terms is generated based on GO tree topology, which is then used to cluster genes with 'binary cut' [139]. The functional characteristics of

each cluster is then displayed with a word cloud. Accordingly, we used the *simplifyEnrichment* with the 'Relevance' measure of similarity to calculate semantic similarity and display the dominant biological processes and molecular functions enriched in the maternal and adult complements, each phase of the MZT, and each life [139,140].

Expression of Key Developmental and Epigenetic Biomarkers

While WGCNA provides a global view of gene expression dynamics during the MZT, examining enzymatic expression of key MZT biomarkers provides a more detailed view of this process. In light of this, we examined the expression of enzymes linked to maternal transcript degradation (Cyclin-B, and Smaug), suppression of zygotic transcription (Kaiso), and zygotic genome activation (Sox2, Wnt8, and TBXT), as well as the expression of enzymes that provide transcriptional regulation capacity during the MZT (DNMT1, DNMT3A, TET1, MBD2, MBD3, UHRF1, and BRG1). A local alignment search of the *M. capitata* transcriptome was used to find the enzymes of interest for expression analysis [69,73]. Anthozoan (as available) and model organism protein sequences for selected enzymes were identified from the NCBI protein database for query. Sequence length, organism, quality, and date modified were considered in cases for which there were multiple available sequences. *Blastx* was used to identify the enzymes of interest in the *M. capitata* reference transcriptome (e-value < 10−5, max_target_seqs=100) using a Blast database created from the predicted cDNA sequences [69]. The hits table was filtered for duplicates in R. This table was used to subset the vst-normalized gene counts matrix, leaving only hits to

the enzymes of interest. The top ten hits for each enzyme are reported in Table S8. The top hits for each enzyme generally exhibited much higher bitscores and lower e-values compared to subsequent hits. However, in some cases, the blast results and expression profiles for the top 2-3 hits were nearly identical, even though the genes were located on different scaffolds in the genome. Due to the robust alignment of the top hits to the *M. capitata* genome, and the similar expression profiles of comparable hits, vst-transformed expression was plotted only for each enzyme's top hit. In plotting the expression of these developmental and epigenetic biomarkers, we gain further support on the timeline of and the epigenetic state necessary for the MZT.

The expression profiles of the top developmental and epigenetic enzymes are supported with differential expression analysis. To test for changes in expression between subsequent timepoints, a DESeq2 dataframe was first constructed using all genes that passed the *pOverA* (*pOverA* 0.083, 10) filter described above [134,135]. Differential expression analysis was then performed on filtered counts using the Wald model to estimate pairwise differences in gene expression between subsequent life stages [135]. Finally, significant changes in the expression of the developmental and epigenetic biomarkers were extracted from the DESeq2 results, by filtering for the top hits for each enzyme and applying a cut-off of >|1| logfoldchange and padj<0.05 (Table S8). These results indicate when transcriptional regulation occurs for these key enzymes, providing further support for their activity during the early development of *M. capitata*.

Declarations

Ethics approval and consent to participate

Not applicable

Consent for publication

Not applicable

Availability of data and materials

All raw data generated for this project has been deposited in the NCBI repository and can be accessed with Bioproject accession IDs, PRJNA731596 (adult) and PRJNA616341 (all other timepoints). Additionally, all code used for transcriptomic analysis is publicly accessible from the GitHub repository, Mcapitata_Developmental_Gene_Expression_Timeseries, which will be submitted for a DOI on Zenodo upon acceptance for publication.

Competing interests

The authors declare that they have no competing interests.

Funding

This work was funded by BSF grant 2016321 to HMP and TM. This work was also partially supported by the USDA National Institute of Food and Agriculture, Hatch Formula project accession number 1017848.

Authors' contributions

HMP and TM designed and provided financial support for the study; ES MN, VS, MS, and HMP conducted the field work and collected the samples; EC conducted the molecular work; EC and HMP analyzed the data; EC, HMP, and ES wrote the manuscript, all authors contributed to the final manuscript.

Acknowledgements

We dedicate this work to our colleague and friend Dr. Diane Adams. We would like to thank the faculty and staff of the Hawai‘i Institute of Marine Biology and the University of Rhode Island Computing.

References

1. Hughes TP, Barnes ML, Bellwood DR, Cinner JE, Cumming GS, Jackson JBC, et al. Coral reefs in the Anthropocene. Nature. 2017;546:82–90.

2. Hughes TP, Tanner JE. Recruitment failure, life histories, and long-term decline of Caribbean corals. Ecology. Wiley Online Library; 2000;81:2250–63.

3. Cowen RK, Sponaugle S. Larval Dispersal and Marine Population Connectivity. Ann Rev Mar Sci. Annual Reviews; 2009;1:443–66.

4. Ritson-Williams R, Arnold SN, Fogarty ND, Steneck RS, Vermeij MJA, Paul VJ. New perspectives on ecological mechanisms affecting coral recruitment on reefs. Smithson Contrib Mar Sci. 2009;38:437.

5. Connell JH. Disturbance and recovery of coral assemblages [Internet]. 1997 p. 101–13. Available from: https://link.springer.com/content/pdf/10.1007/s003380050246.pdf

6. Byrne M. Global change ecotoxicology: Identification of early life history bottlenecks in marine invertebrates, variable species responses and variable experimental approaches. Mar Environ Res. 2012;76:3–15.

7. Przeslawski R, Byrne M, Mellin C. A review and meta-analysis of the effects of multiple abiotic stressors on marine embryos and larvae. Glob Chang Biol. 2015;21:2122–40.

8. Byrne M, Przeslawski R. Multistressor impacts of warming and acidification of the ocean on marine invertebrates' life histories. Integr Comp Biol. 2013;53:582–96.

9. Baird AH, Guest JR, Willis BL. Systematic and Biogeographical Patterns in the Reproductive Biology of Scleractinian Corals. Annu Rev Ecol Evol Syst. Annual Reviews; 2009;40:551–71.

10. Harrison PL. Sexual Reproduction of Scleractinian Corals. In: Dubinsky Z, Stambler N, editors. Coral Reefs: An Ecosystem in Transition. Dordrecht: Springer Netherlands; 2011. p. 59–85.

11. Wilson JR, Harrison PL. Settlement-competency periods of larvae of three species of scleractinian corals. Mar Biol. 1998;131:339–45.

12. Albright R, Mason B. Projected near-future levels of temperature and pCO2 reduce coral fertilization success. PLoS One. 2013;8:e56468.

13. Albright R, Mason B, Miller M, Langdon C. Ocean acidification compromises recruitment success of the threatened Caribbean coral Acropora palmata. Proceedings of the National Academy of Sciences. 2010;107:20400–4.

14. Yuan X, Yuan T, Huang H, Jiang L, Zhou W, Liu S. Elevated CO 2 delays the early development of scleractinian coral Acropora gemmifera. Sci Rep [Internet]. Springer US; 2018;8. Available from: http://dx.doi.org/10.1038/s41598-018-21267-3

15. Albright R, Langdon C. Ocean acidification impacts multiple early life history processes of the Caribbean coral Porites astreoides. Glob Chang Biol. Wiley/Blackwell (10.1111); 2011;17:2478–87.

16. Nakamura M, Ohki S, Suzuki A, Sakai K. Coral larvae under ocean acidification: Survival, metabolism, and metamorphosis. PLoS One [Internet]. 2011;6. Available from: http://dx.doi.org/10.1371/journal.pone.0014521

17. Rivest EB, Hofmann GE. Responses of the metabolism of the larvae of Pocillopora damicornis to ocean acidification and warming. PLoS One [Internet]. 2014;9. Available from: http://dx.doi.org/10.1371/journal.pone.0096172

18. Byrne M, Ho M, Selvakumaraswamy P, Nguyen HD, Dworjanyn SA, Davis AR. Temperature, but not pH, compromises sea urchin fertilization and early development under near-future climate change scenarios. Proc Biol Sci. royalsocietypublishing.org; 2009;276:1883–8.

19. Ericson JA, Lamare MD, Morley SA, Barker MF. The response of two ecologically important Antarctic invertebrates (Sterechinus neumayeri and Parborlasia corrugatus) to reduced seawater pH: effects on fertilisation and embryonic development. Mar Biol. 2010;157:2689–702.

20. Ericson JA, Ho MA, Miskelly A, King CK, Virtue P. Combined effects of two

ocean change stressors, warming and acidification, on fertilization and early development of the Antarctic echinoid Sterechinus …. Polar Biol [Internet]. Springer; 2012; Available from: https://sci-hub.do/https://idp.springer.com/authorize/casa?redirect_uri=https://link.springer.com/article/10.1007/s00300-011-1150-7&casa_token=K9-6id_XO1MAAAAA:lRiksA1G-leVEoWnBTYp3P_XBOEyLXeyc7TIF9PiZXgsLbFqcrzfGlBlJA7RBZLE1OL1EEh_sZXdUseYGQ

21. Foo SA, Dworjanyn SA, Poore AGB, Byrne M. Adaptive capacity of the habitat modifying sea urchin Centrostephanus rodgersii to ocean warming and ocean acidification: performance of early embryos. PLoS One. 2012;7:e42497.

22. Dahlke FT, Lucassen M, Bickmeyer U, Wohlrab S, Puvanendran V, Mortensen A, et al. Fish embryo vulnerability to combined acidification and warming coincides with a low capacity for homeostatic regulation. J Exp Biol [Internet]. 2020;223. Available from: http://dx.doi.org/10.1242/jeb.212589

23. Stitzel ML, Seydoux G. Regulation of the oocyte-to-zygote transition. Science. 2007;316:407–8.

24. Hamdoun A, Epel D. Embryo stability and vulnerability in an always changing world. Proc Natl Acad Sci U S A. 2007;104:1745–50.

25. Ahi EP, Singh P, Lecaudey LA, Gessl W, Sturmbauer C. Maternal mRNA input of growth and stress-response-related genes in cichlids in relation to egg size and trophic specialization. Evodevo. 2018;9:23.

26. Liu MM, Davey JW, Jackson DJ, Blaxter ML, Davison A. A conserved set of maternal genes? Insights from a molluscan transcriptome. Int J Dev Biol. 2014;58:501–11.

27. Romney AL, Podrabsky JE. Transcriptomic analysis of maternally provisioned cues for phenotypic plasticity in the annual killifish, Austrofundulus limnaeus. Evodevo. 2017;8:6.

28. Bernier C, Boidin-Wichlacz C, Tasiemski A, Hautekèete N, Massol F, Cuvillier-Hot V. Transgenerational Immune Priming in the Field: Maternal Environmental Experience Leads to Differential Immune Transfer to Oocytes in the Marine Annelid Hediste diversicolor. Genes [Internet]. 2019;10. Available from: http://dx.doi.org/10.3390/genes10120989

29. Mommens M, Fernandes JMO, Tollefsen KE, Johnston IA, Babiak I. Profiling of the embryonic Atlantic halibut (Hippoglossus hippoglossus L.) transcriptome reveals maternal transcripts as potential markers of embryo quality. BMC Genomics. 2014;15:829.

30. Amiri E, Herman JJ, Strand MK, Tarpy DR, Rueppell O. Egg transcriptome profile responds to maternal virus infection in honey bees, Apis mellifera. Infect Genet

Evol. 2020;85:104558.

31. Kim C-H, Kim EJ, Seo C, Nam YK. Transcriptome Analysis of Maternal Gene Transcripts in Unfertilized Eggs of Misgurnus anguillicaudatus and Identification of Immune-Related Maternal Genes. Int J Mol Sci [Internet]. 2020;21. Available from: http://dx.doi.org/10.3390/ijms21113872

32. Davidson PL, Thompson JW, Foster MW, Moseley MA, Byrne M, Wray GA. A comparative analysis of egg provisioning using mass spectrometry during rapid life history evolution in sea urchins. Evol Dev. 2019;21:188–204.

33. Van Etten J, Shumaker A, Mass T, Putnam HM, Bhattacharya D. Transcriptome analysis provides a blueprint of coral egg and sperm functions [Internet]. PeerJ. 2020. p. e9739. Available from: http://dx.doi.org/10.7717/peerj.9739

34. Reyes-Bermudez A, Villar-Briones A, Ramirez-Portilla C, Hidaka M, Mikheyev AS. Developmental Progression in the Coral Acropora digitifera Is Controlled by Differential Expression of Distinct Regulatory Gene Networks. Genome Biol Evol. 2016;8:851–70.

35. Strader M, Aglyamova G, Matz M. Molecular characterization of larval development from fertilization to metamorphosis in a reef-building coral. BMC Genomics. 2018;19:1–17.

36. Chan WY, Chung J, Peplow LM, Hoffmann AA, van Oppen MJH. Maternal effects in gene expression of interspecific coral hybrids. Mol Ecol. 2021;30:517–27.

37. Dahlke FT, Leo E, Mark FC, Pörtner H-O, Bickmeyer U, Frickenhaus S, et al. Effects of ocean acidification increase embryonic sensitivity to thermal extremes in Atlantic cod, Gadus morhua. Glob Chang Biol. 2017;23:1499–510.

38. Michalek-Wagner K, Willis BL. Impacts of bleaching on the soft coral Lobophytum compactum. II. Biochemical changes in adults and their eggs [Internet]. Coral Reefs. 2001. p. 240–6. Available from: http://dx.doi.org/10.1007/pl00006959

39. Tadros W, Lipshitz HD. The maternal-to-zygotic transition: a play in two acts. Development. 2009;136:3033–42.

40. Vastenhouw NL, Cao WX, Lipshitz HD. The maternal-to-zygotic transition revisited. Development [Internet]. 2019;146. Available from: http://dx.doi.org/10.1242/dev.161471

41. Wu E, Vastenhouw NL. From mother to embryo: A molecular perspective on zygotic genome activation. Current Topics in Developmental Biology. Academic Press; 2020.

42. Despic V, Neugebauer KM. RNA tales – how embryos read and discard messages from mom [Internet]. Journal of Cell Science. 2018. p. jcs201996. Available from:

http://dx.doi.org/10.1242/jcs.201996

43. Hamm DC, Harrison MM. Regulatory principles governing the maternal-to-zygotic transition: insights from Drosophila melanogaster. Open Biol. 2018;8:180183.

44. Bazzini AA, Viso F, Moreno-Mateos MA, Johnstone TG, Vejnar CE, Qin Y, et al. Codon identity regulates mRNA stability and translation efficiency during the maternal-to-zygotic transition. EMBO J. EMBO; 2016;35:2087–103.

45. Chen L, Dumelie JG, Li X, Cheng MH, Yang Z, Laver JD, et al. Global regulation of mRNA translation and stability in the early Drosophila embryo by the Smaug RNA-binding protein. Genome Biol. 2014;15:R4.

46. Tadros W, Goldman AL, Babak T, Menzies F, Vardy L, Orr-Weaver T, et al. SMAUG is a major regulator of maternal mRNA destabilization in Drosophila and its translation is activated by the PAN GU kinase. Dev Cell. 2007;12:143–55.

47. Ruzov A, Savitskaya E, Hackett JA, Reddington JP, Prokhortchouk A, Madej MJ, et al. The non-methylated DNA-binding function of Kaiso is not required in early Xenopus laevis development. Development. 2009;136:729–38.

48. Ruzov A, Dunican DS, Prokhortchouk A, Pennings S, Stancheva I, Prokhortchouk E, et al. Kaiso is a genome-wide repressor of transcription that is essential for amphibian development. Development. 2004;131:6185–94.

49. Li L, Lu X, Dean J. The maternal to zygotic transition in mammals. Mol Aspects Med. 2013;34:919–38.

50. Lee MT, Bonneau AR, Takacs CM, Bazzini AA, DiVito KR, Fleming ES, et al. Nanog, Pou5f1 and SoxB1 activate zygotic gene expression during the maternal-to-zygotic transition. Nature. 2013;503:360–4.

51. Benoit B, He CH, Zhang F, Votruba SM, Tadros W, Westwood JT, et al. An essential role for the RNA-binding protein Smaug during the Drosophila maternal-to-zygotic transition. Development. 2009;136:923–32.

52. Scholz CB, Technau U. The ancestral role of Brachyury: expression of NemBra1 in the basal cnidarian Nematostella vectensis (Anthozoa). Dev Genes Evol. 2003;212:563–70.

53. Gentsch GE, Spruce T, Owens NDL, Smith JC. Maternal pluripotency factors initiate extensive chromatin remodelling to predefine first response to inductive signals. Nat Commun. 2019;10:4269.

54. Smith J, Theodoris C, Davidson EH. A gene regulatory network subcircuit drives a dynamic pattern of gene expression. Science. 2007;318:794–7.

55. Potok ME, Nix DA, Parnell TJ, Cairns BR. Reprogramming the maternal zebrafish

genome after fertilization to match the paternal methylation pattern. Cell. 2013;153:759–72.

56. Byrne M, Foo SA, Ross PM, Putnam HM. Limitations of cross- and multigenerational plasticity for marine invertebrates faced with global climate change [Internet]. Global Change Biology. 2020. p. 80–102. Available from: http://dx.doi.org/10.1111/gcb.14882

57. Eirin-Lopez JM, Putnam HM. Marine Environmental Epigenetics. 2018; Available from: https://doi.org/10.1146/annurev-marine-010318-

58. Howell CY, Bestor TH, Ding F, Latham KE, Mertineit C, Trasler JM, et al. Genomic imprinting disrupted by a maternal effect mutation in the Dnmt1 gene. Cell. 2001;104:829–38.

59. Ito S, Shen L, Dai Q, Wu SC, Collins LB, Swenberg JA, et al. Tet proteins can convert 5-methylcytosine to 5-formylcytosine and 5-carboxylcytosine. Science. 2011;333:1300–3.

60. Stancheva I, Meehan RR. Transient depletion of xDnmt1 leads to premature gene activation in Xenopus embryos. Genes Dev. 2000;14:313–27.

61. Bostick M, Kim JK, Estève P-O, Clark A, Pradhan S, Jacobsen SE. UHRF1 plays a role in maintaining DNA methylation in mammalian cells. Science. 2007;317:1760–4.

62. Bird AP, Wolffe AP. Methylation-induced repression—belts, braces, and chromatin. Cell. Elsevier; 1999;99:451–4.

63. Hendrich B, Abbott C, McQueen H, Chambers D, Cross S, Bird A. Genomic structure and chromosomal mapping of the murine and human Mbd1, Mbd2, Mbd3, and Mbd4 genes. Mamm Genome. 1999;10:906–12.

64. Hendrich B, Guy J, Ramsahoye B, Wilson VA, Bird A. Closely related proteins MBD2 and MBD3 play distinctive but interacting roles in mouse development. Genes Dev. 2001;15:710–23.

65. Bultman SJ, Gebuhr TC, Pan H, Svoboda P, Schultz RM, Magnuson T. Maternal BRG1 regulates zygotic genome activation in the mouse. Genes Dev. 2006;20:1744–54.

66. Padilla-Gamiño JL, Weatherby TM, Waller RG, Gates RD. Formation and structural organization of the egg-sperm bundle of the scleractinian coral Montipora capitata. Coral Reefs. 2011;30:371–80.

67. Padilla-Gamiño JL, Gates RD. Spawning dynamics in the Hawaiian reef-building coral Montipora capitata. Mar Ecol Prog Ser. 2012;449:145–60.

68. Okubo N, Mezaki T, Nozawa Y, Nakano Y, Lien YT, Fukami H, et al. Comparative embryology of eleven species of stony corals (Scleractinia). PLoS One [Internet]. 2013;8. Available from: http://dx.doi.org/10.1371/journal.pone.0084115

69. Shumaker A, Putnam HM, Qiu H, Price DC, Zelzion E, Harel A, et al. Genome analysis of the rice coral Montipora capitata. Sci Rep. Nature Publishing Group; 2019;9:2571.

70. Buchfink B, Xie C, Huson DH. Fast and sensitive protein alignment using DIAMOND. Nat Methods. 2015;12:59–60.

71. Jones P, Binns D, Chang H-Y, Fraser M, Li W, McAnulla C, et al. InterProScan 5: genome-scale protein function classification. Bioinformatics. 2014;30:1236–40.

72. Götz S, García-Gómez JM, Terol J, Williams TD, Nagaraj SH, Nueda MJ, et al. High-throughput functional annotation and data mining with the Blast2GO suite. Nucleic Acids Res. 2008;36:3420–35.

73. UniProt Consortium. UniProt: a worldwide hub of protein knowledge. Nucleic Acids Res. 2019;47:D506–15.

74. Wong JM, Gaitán-Espitia JD, Hofmann GE. Transcriptional profiles of early stage red sea urchins (Mesocentrotus franciscanus) reveal differential regulation of gene expression across development. Mar Genomics. 2019;48:100692.

75. Gildor T, Malik A, Sher N, Avraham L, Ben-Tabou de-Leon S. Quantitative developmental transcriptomes of the Mediterranean sea urchin Paracentrotus lividus. Mar Genomics. 2016;25:89–94.

76. Heyland A, Vue Z, Voolstra CR, Medina M, Moroz LL. Developmental transcriptome of Aplysia californica'. J Exp Zool B Mol Dev Evol. Wiley Online Library; 2011;316:113–34.

77. Lim DS, Hasty P. A mutation in mouse rad51 results in an early embryonic lethal that is suppressed by a mutation in p53 [Internet]. Molecular and Cellular Biology. 1996. p. 7133–43. Available from: http://dx.doi.org/10.1128/mcb.16.12.7133

78. Ludwig DL, MacInnes MA, Takiguchi Y, Purtymun PE, Henrie M, Flannery M, et al. A murine AP-endonuclease gene-targeted deficiency with post-implantation embryonic progression and ionizing radiation sensitivity. Mutat Res. 1998;409:17–29.

79. Heyer BS, MacAuley A, Behrendtsen O, Werb Z. Hypersensitivity to DNA damage leads to increased apoptosis during early mouse development. Genes Dev. 2000;14:2072–84.

80. Baird AH, Yakovleva IM, Harii S, Sinniger F, Hidaka M. Environmental constraints on the mode of symbiont transmission in corals. J Exp Mar Bio Ecol. 2021;151499.

81. Epel D, Hemela K, Shick M, Patton C. Development in the floating world: defenses of eggs and embryos against damage from UV radiation. Am Zool. Oxford University Press UK; 1999;39:271–8.

82. Willis J, DeStephanis D, Patel Y, Gowda V, Yan S. Study of the DNA damage checkpoint using Xenopus egg extracts. J Vis Exp. 2012;e4449.

83. Malloy KD, Holman MA, Mitchell D, Detrich HW 3rd. Solar UVB-induced DNA damage and photoenzymatic DNA repair in antarctic zooplankton. Proc Natl Acad Sci U S A. 1997;94:1258–63.

84. Vetter RD, Kurtzman A, Mori T. Diel cycles of DNA damage and repair in eggs and larvae of northern anchovy, Engraulis mordax, exposed to solar ultraviolet radiation. Photochem Photobiol. Wiley; 1999;69:27–33.

85. Ménézo Y, Dale B, Cohen M. DNA damage and repair in human oocytes and embryos: a review. Zygote. 2010;18:357–65.

86. Yu S-L, Lee S-K. Ultraviolet radiation: DNA damage, repair, and human disorders. Mol Cell Toxicol. Springer Science and Business Media LLC; 2017;13:21–8.

87. Cadet J, Wagner JR. DNA base damage by reactive oxygen species, oxidizing agents, and UV radiation. Cold Spring Harb Perspect Biol [Internet]. 2013;5. Available from: http://dx.doi.org/10.1101/cshperspect.a012559

88. Heyward AJ. Sexual reproduction in five species of the coral Montipora. Hawaii Institute of Marine Biology, Technical Report. 1986;37:170–8.

89. Nesa B, Baird AH, Harii S, Yakovleva I, Hidaka M. Algal symbionts increase DNA damage in coral planulae exposed to sunlight. Zool Stud. Academia Sinica; 2012;51:6.

90. Reef R, Dunn S, Levy O, Dove S, Shemesh E, Brickner I, et al. Photoreactivation is the main repair pathway for UV-induced DNA damage in coral planulae. J Exp Biol. 2009;212:2760–6.

91. Muller-Parker G, D'Elia CF, Cook CB. Interactions Between Corals and Their Symbiotic Algae. In: Birkeland C, editor. Coral Reefs in the Anthropocene. Dordrecht: Springer Netherlands; 2015. p. 99–116.

92. Barckmann B, Simonelig M. Control of maternal mRNA stability in germ cells and early embryos. Biochim Biophys Acta. 2013;1829:714–24.

93. Laver JD, Marsolais AJ, Smibert CA, Lipshitz HD. Chapter Two - Regulation and Function of Maternal Gene Products During the Maternal-to-Zygotic Transition in Drosophila. In: Lipshitz HD, editor. Current Topics in Developmental Biology. Academic Press; 2015. p. 43–84.

94. Runft LL, Jaffe LA, Mehlmann LM. Egg activation at fertilization: where it all begins. Dev Biol. 2002;245:237–54.

95. Coward K, Bromage NR, Hibbitt O, Parrington J. Gamete physiology, fertilization and egg activation in teleost fish. Rev Fish Biol Fish. Springer; 2002;12:33–58.

96. Harvey SA, Sealy I, Kettleborough R, Fenyes F, White R, Stemple D, et al. Identification of the zebrafish maternal and paternal transcriptomes. Development. 2013;140:2703–10.

97. Collart C, Owens NDL, Bhaw-Rosun L, Cooper B, De Domenico E, Patrushev I, et al. High-resolution analysis of gene activity during the Xenopus mid-blastula transition [Internet]. Development. 2014. p. 1927–39. Available from: http://dx.doi.org/10.1242/dev.102012

98. Helm RR, Siebert S, Tulin S, Smith J, Dunn CW. Characterization of differential transcript abundance through time during Nematostella vectensis development. BMC Genomics. 2013;14:266.

99. Rowicka M, Kudlicki A, Tu BP, Otwinowski Z. High-resolution timing of cell cycle-regulated gene expression. Proc Natl Acad Sci U S A. 2007;104:16892–7.

100. Audic Y, Anderson C, Bhatty R, Hartley RS. Zygotic regulation of maternal cyclin A1 and B2 mRNAs. Mol Cell Biol. 2001;21:1662–71.

101. Audic Y, Garbrecht M, Fritz B, Sheets MD, Hartley RS. Zygotic control of maternal cyclin A1 translation and mRNA stability. Dev Dyn. Wiley Online Library; 2002;225:511–21.

102. Beddington RS, Rashbass P, Wilson V. Brachyury--a gene affecting mouse gastrulation and early organogenesis. Dev Suppl. 1992;157–65.

103. Herrmann BG, Labeit S, Poustka A, King TR, Lehrach H. Cloning of the T gene required in mesoderm formation in the mouse. Nature. 1990;343:617–22.

104. Fritzenwanker JH, Genikhovich G, Kraus Y, Technau U. Early development and axis specification in the sea anemone Nematostella vectensis. Dev Biol. 2007;310:264–79.

105. Kraus YA, Markov AV. Gastrulation in Cnidaria: The key to an understanding of phylogeny or the chaos of secondary modifications? Biol Bull Rev. Pleiades Publishing Ltd; 2017;7:7–25.

106. Putnam HM. Avenues of reef-building coral acclimatization in response to rapid environmental change. J Exp Biol [Internet]. 2021;224. Available from: http://dx.doi.org/10.1242/jeb.239319

107. Levitan S, Sher N, Brekhman V, Ziv T, Lubzens E, Lotan T. The making of an

embryo in a basal metazoan: Proteomic analysis in the sea anemone Nematostella vectensis. Proteomics. 2015;15:4096–104.

108. Yagound B, Remnant EJ, Buchmann G, Oldroyd BP. Intergenerational transfer of DNA methylation marks in the honey bee. Proc Natl Acad Sci U S A [Internet]. 2020; Available from: http://dx.doi.org/10.1073/pnas.2017094117

109. Xu X, Li G, Li C, Zhang J, Wang Q, Simmons DK, et al. Evolutionary transition between invertebrates and vertebrates via methylation reprogramming in embryogenesis. Natl Sci Rev. Oxford Academic; 2019;6:993–1003.

110. Liew YJ, Howells EJ, Wang X, Michell CT, Burt JA, Idaghdour Y, et al. Intergenerational epigenetic inheritance in reef-building corals. Nat Clim Chang. 2020;10:254–9.

111. Harris KD, Lloyd JPB, Domb K, Zilberman D, Zemach A. DNA methylation is maintained with high fidelity in the honey bee germline and exhibits global non-functional fluctuations during somatic development. Epigenetics Chromatin. 2019;12:62.

112. Hales BF, Grenier L, Lalancette C, Robaire B. Epigenetic programming: from gametes to blastocyst. Birth Defects Res A Clin Mol Teratol. 2011;91:652–65.

113. Okano M, Bell DW, Haber DA, Li E. DNA methyltransferases Dnmt3a and Dnmt3b are essential for de novo methylation and mammalian development. Cell. Elsevier; 1999;99:247–57.

114. de Mendoza A, Lister R, Bogdanovic O. Evolution of DNA Methylome Diversity in Eukaryotes. J Mol Biol [Internet]. 2019; Available from: http://dx.doi.org/10.1016/j.jmb.2019.11.003

115. de Mendoza A, Hatleberg WL, Pang K, Leininger S, Bogdanovic O, Pflueger J, et al. Convergent evolution of a vertebrate-like methylome in a marine sponge. Nat Ecol Evol. 2019;3:1464–73.

116. Potok ME, Nix DA, Parnell TJ, Cairns BR. Germline epigenetics, and reprogramming in zebrafish early embryos. Epigenetics Chromatin. 2013;6:O23.

117. Zenk F, Loeser E, Schiavo R, Kilpert F, Bogdanović O, Iovino N. Germ line–inherited H3K27me3 restricts enhancer function during maternal-to-zygotic transition. Science. American Association for the Advancement of Science; 2017;357:212–6.

118. Riviere G, Wu G-C, Fellous A, Goux D, Sourdaine P, Favrel P. DNA Methylation Is Crucial for the Early Development in the Oyster C. gigas [Internet]. Marine Biotechnology. 2013. p. 739–53. Available from: http://dx.doi.org/10.1007/s10126-013-9523-2

119. Li Y, Zhang L, Li Y, Li W, Guo Z, Li R, et al. Dynamics of DNA Methylation

and DNMT Expression During Gametogenesis and Early Development of Scallop Patinopecten yessoensis. Mar Biotechnol . 2019;21:196–205.

120. Murphy PJ, Wu SF, James CR, Wike CL, Cairns BR. Placeholder Nucleosomes Underlie Germline-to-Embryo DNA Methylation Reprogramming. Cell. 2018;172:993–1006.e13.

121. Hershko AY, Kafri T, Fainsod A, Razin A. Methylation of HoxA5 and HoxB5 and its relevance to expression during mouse development. Gene. 2003;302:65–72.

122. Jokiel PL, Hildemann WH, Bigger CH. Clonal Population Structure of Two Sympatric Species of the Reef Coral Montipora. Bull Mar Sci. 1983;33:181–7.

123. Jokiel PL, Brown EK, Friedlander A, Ku'ulei Rodgers S, Smith WR. Hawai'i Coral Reef Assessment and Monitoring Program: Spatial Patterns and Temporal Dynamics in Reef Coral Communities. Pac Sci. University of Hawai'i Press; 2004;58:159–74.

124. Padilla-Gamiño JL, Pochon X, Bird C, Concepcion GT, Gates RD. From Parent to Gamete: Vertical Transmission of Symbiodinium (Dinophyceae) ITS2 Sequence Assemblages in the Reef Building Coral Montipora capitata. Ferse SCA, editor. PLoS One. 2012;7:e38440.

125. Gibbin EM, Putnam HM, Gates RD, Nitschke MR, Davy SK. Species-specific differences in thermal tolerance may define susceptibility to intracellular acidosis in reef corals. Mar Biol. Springer Verlag; 2015;162:717–23.

126. Jimenez IM, Kühl M, Larkum AWD, Ralph PJ. Effects of flow and colony morphology on the thermal boundary layer of corals. J R Soc Interface. royalsocietypublishing.org; 2011;8:1785–95.

127. Andrews S, Others. FastQC: a quality control tool for high throughput sequence data. Babraham Bioinformatics, Babraham Institute, Cambridge, United Kingdom; 2010.

128. Ewels P, Magnusson M, Lundin S, Käller M. MultiQC: summarize analysis results for multiple tools and samples in a single report. Bioinformatics. 2016;32:3047–8.

129. Chen S, Zhou Y, Chen Y, Gu J. fastp: an ultra-fast all-in-one FASTQ preprocessor. Bioinformatics. academic.oup.com; 2018;34:i884–90.

130. Kim D, Paggi JM, Park C, Bennett C, Salzberg SL. Graph-based genome alignment and genotyping with HISAT2 and HISAT-genotype. Nat Biotechnol. 2019;37:907–15.

131. Pertea M, Pertea GM, Antonescu CM, Chang T-C, Mendell JT, Salzberg SL. StringTie enables improved reconstruction of a transcriptome from RNA-seq reads.

Nat Biotechnol. 2015;33:290–5.

132. Pertea GM, Pertea M. GFF Utilities: GffRead and GffCompare. F1000Res [Internet]. Faculty of 1000 Ltd; 2020;9. Available from: https://www.ncbi.nlm.nih.gov/pmc/articles/pmc7222033/

133. Team RC, Others. R: A language and environment for statistical computing. Vienna, Austria; 2013; Available from: https://cran.microsoft.com/snapshot/2014-09-08/web/packages/dplR/vignettes/xdate-dplR.pdf

134. Gentleman R, Carey V, Huber W, Hahne F. genefilter: genefilter: methods for filtering genes from high-throughput experiments, 2017. R package version. 1.

135. Love MI, Huber W, Anders S. Moderated estimation of fold change and dispersion for RNA-seq data with DESeq2. Genome Biol. 2014;15:550.

136. Langfelder P, Horvath S. WGCNA: An R package for weighted correlation network analysis. BMC Bioinformatics [Internet]. 2008;9. Available from: http://dx.doi.org/10.1186/1471-2105-9-559

137. Gu Z. Complexheatmap: Making complex heatmaps. R package version. 2015;1.

138. Young MD, Wakefield MJ, Smyth GK, Oshlack A. Gene ontology analysis for RNA-seq: accounting for selection bias. Genome Biol. 2010;11:R14.

139. Gu Z, Huebschmann D. simplifyEnrichment: an R/Bioconductor package for Clustering and Visualizing Functional Enrichment Results [Internet]. Cold Spring Harbor Laboratory. 2020 [cited 2020 Oct 30]. p. 2020.10.27.312116. Available from: https://www.biorxiv.org/content/10.1101/2020.10.27.312116v1

140. Schlicker A, Domingues FS, Rahnenführer J, Lengauer T. A new measure for functional similarity of gene products based on Gene Ontology. BMC Bioinformatics. 2006;7:302.

Tables and Figures

Figure 1. Timeline of sample collection including example photographs of life each stage.

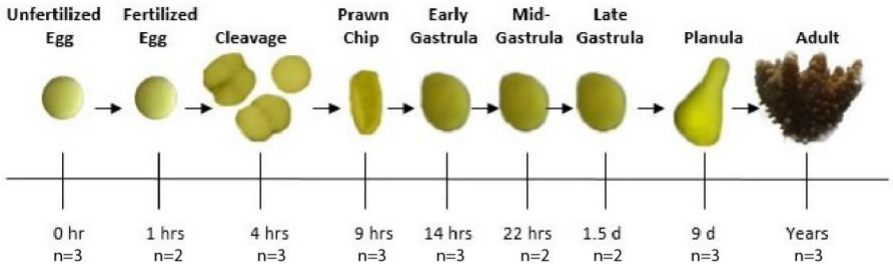

Figure 2. Principal coordinates analysis based on sample-to-sample distance computed from all genes passing a low counts filter, wherein a gene must have a count of 10 or greater in at least 2 out of the 24 samples (pOverA 0.083, 10).

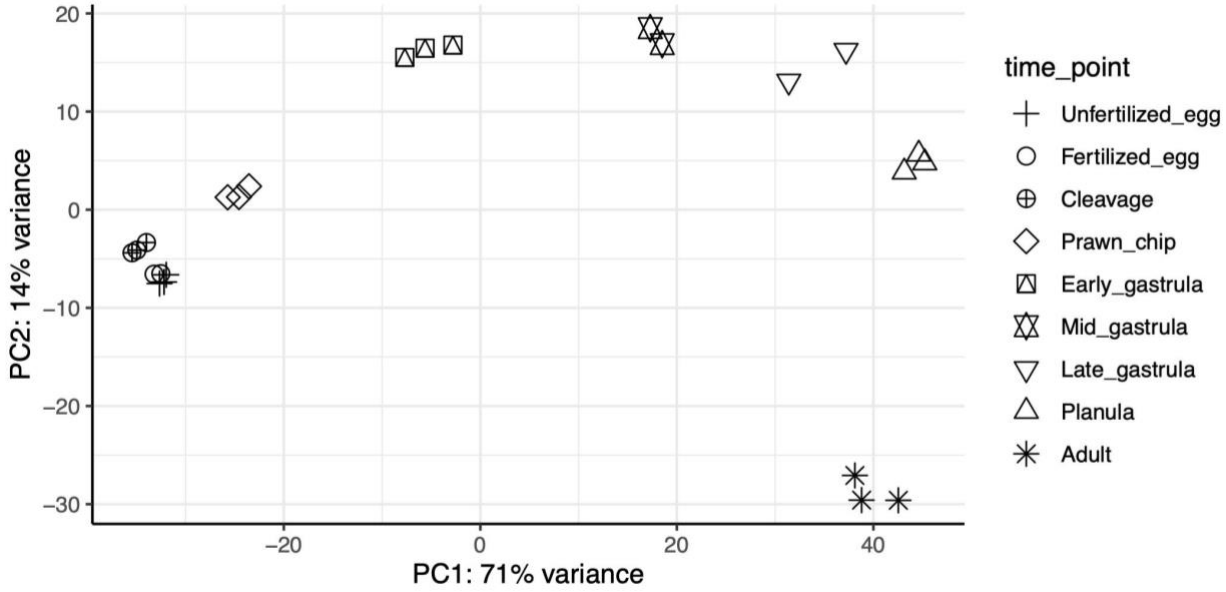

Figure 3. Clustered heatmap of WGCNA module-trait correlations ranging from correlation values of -1 (dark blue) to 0 (white) to +1 (red). Developmental expression clusters are shown on top, while sampled life stages are indicated on bottom. Module clusters 1-9 were identified via a distance matrix computed with *hclust* using module eigengenes.

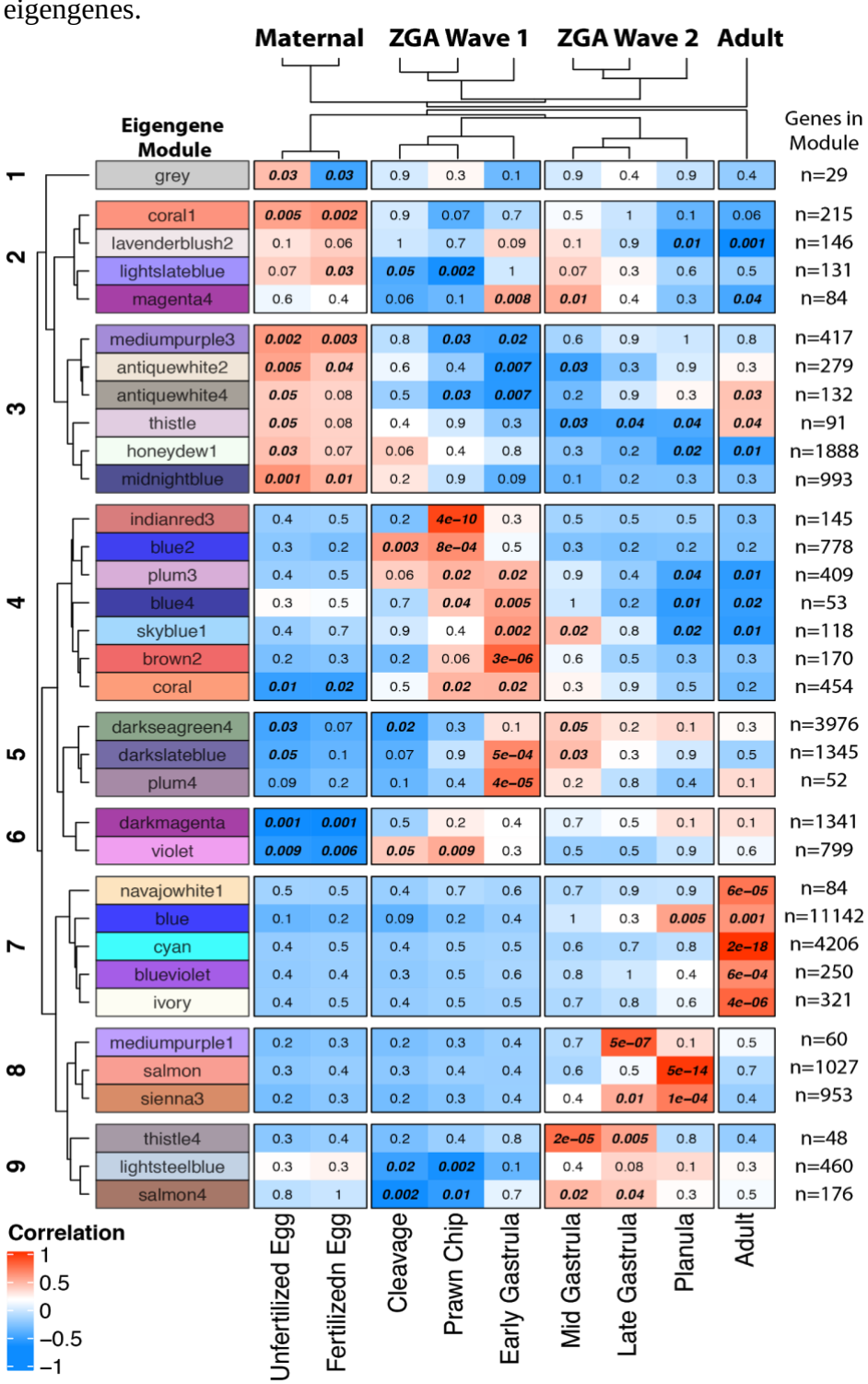

Figure 4. Clustered (binary cut) semantic similarity matrix of Biological Process gene ontology terms for all genes in the 9 modules identified as the A) maternal mRNA complement (n=92 terms), the 11 modules of the B) first wave of the MZT (n=55 terms), and the 10 modules of the C) second wave of the MZT transition (n=22 terms) and the 7 modules of D)"adult" expression (n=31 terms). Terms representing each cluster are shown in a word cloud, with size of term representing frequency of occurrence in the terms. The generic term, "Process" (identified by * in each graphic), was put as a footnote for visual clarity.

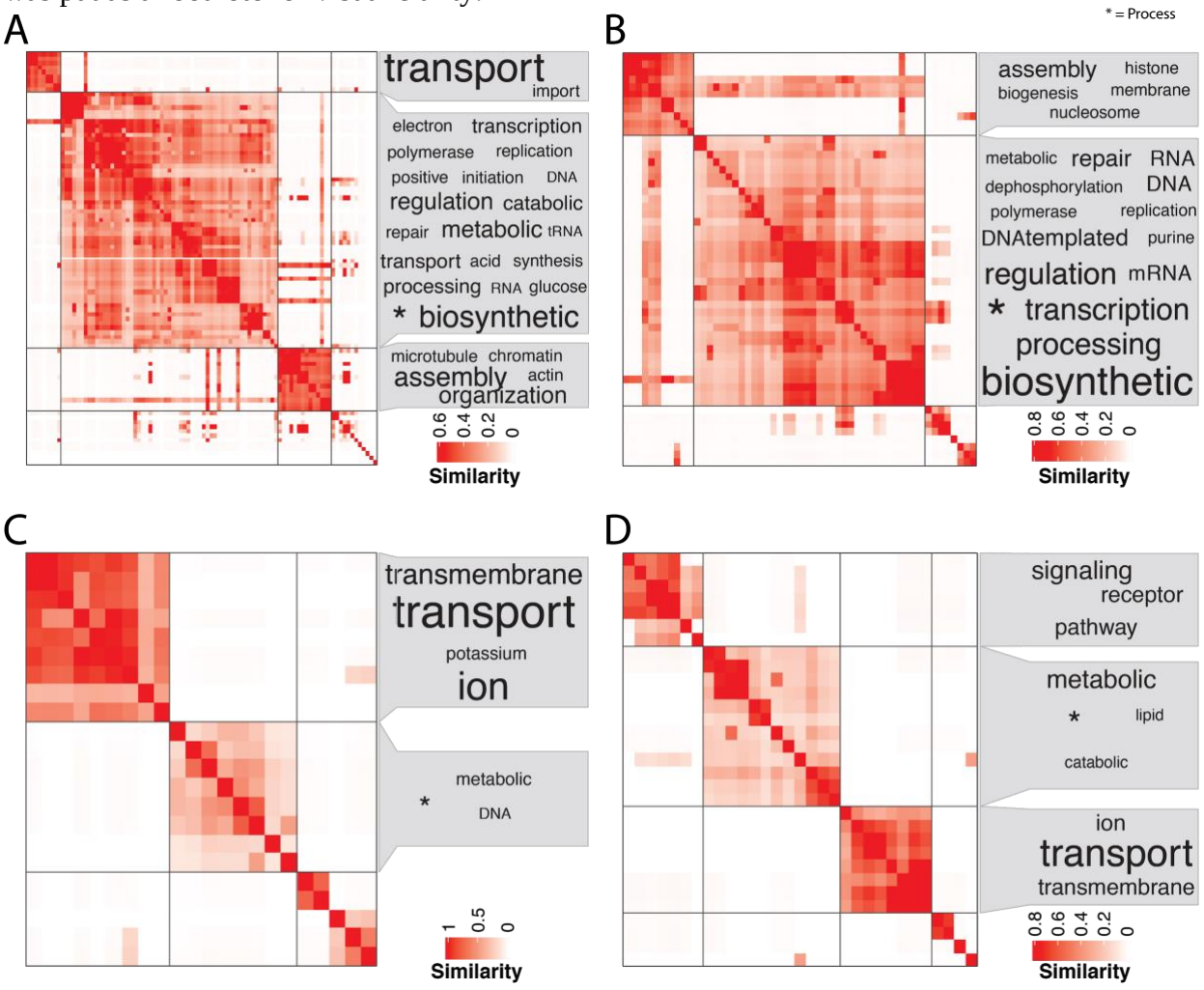

Figure 5. Clustered (binary cut) semantic similarity matrix of Molecular Function gene ontology terms for all genes in the 9 modules identified as the A) maternal mRNA complement (n=92 terms), the 11 modules of the B) first wave of the MZT (n=55 terms), the 10 modules of the C) second wave of the MZT transition (n=22 terms), the 7 modules of the D) "adult" expression (n=31 terms). Terms representing each cluster are shown in a word cloud, with size of term representing frequency of occurrence in the terms. The generic term, "Activity" (identified by * in each graphic), was put as a footnote for visual clarity.

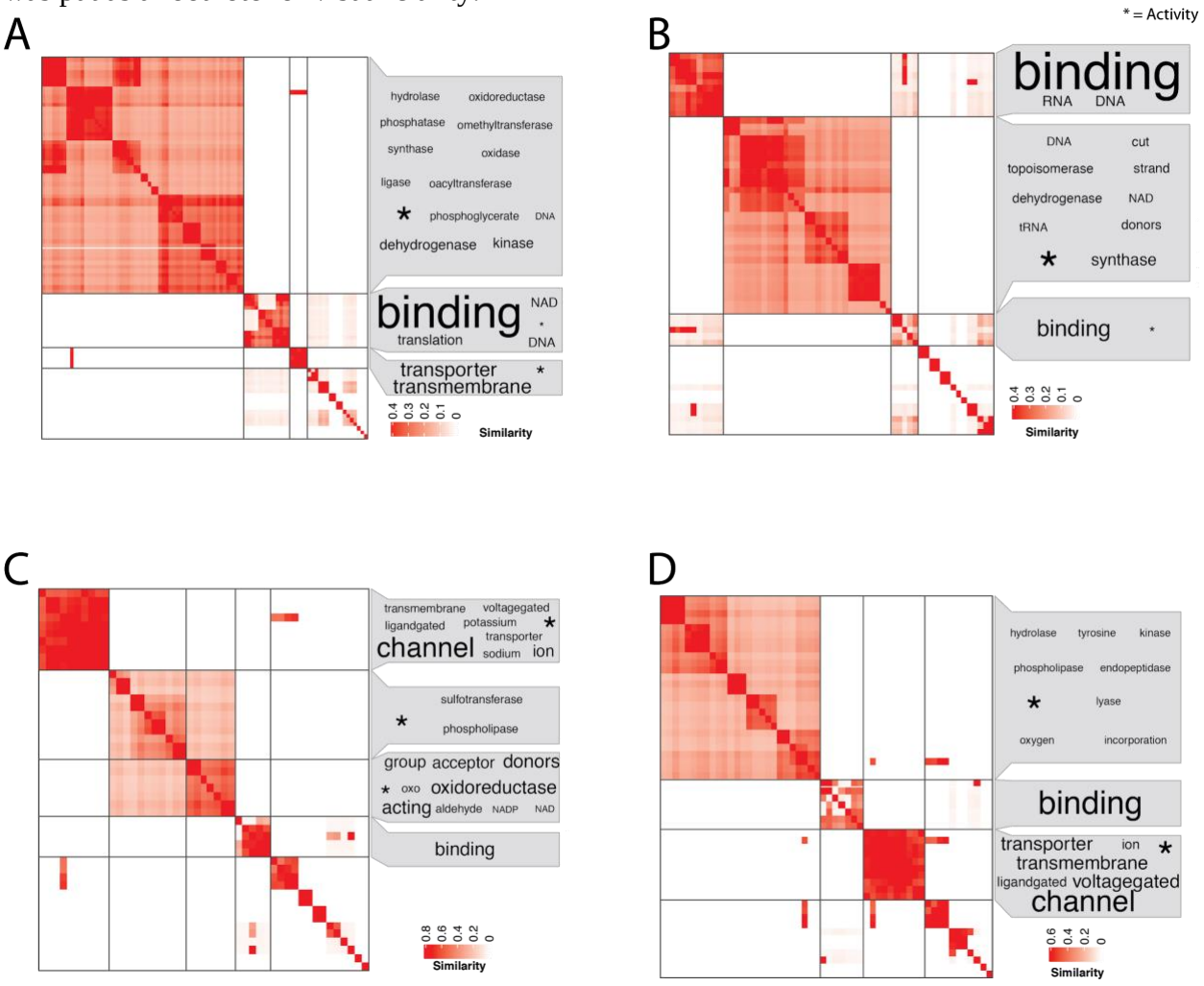

Figure 6. Expression of key biomarkers (M. capitata gene id) in the MZT: i) Cyclin-B (g71356), ii) Smaug (g4639), iii) Kaiso (g60350), iv) Sox2 (g53225), v) Wnt8 (g33149) and vi) Brachyury (TBXT; g68947). Points and error bars display mean±standard error of the mean. Red and blue arrows indicate transitions with significant (padj<0.05, log2FoldChange>|1|) down- and up-regulation, respectively. M=maternal expression, Z=zygotic expression, ZGA=Zygotic genome activation.

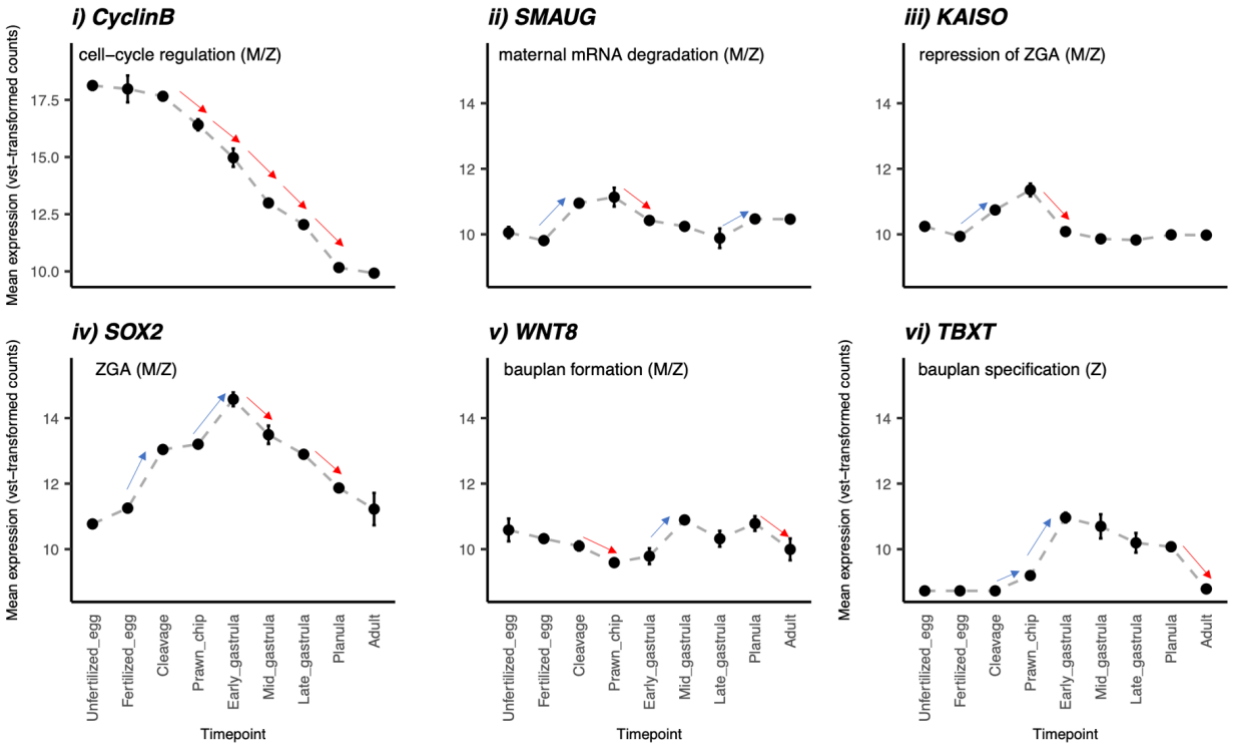

Figure 7. Expression of enzymes (M. capitata gene id) involved with i) DNMT3a (g25804), ii) DNMT1 (g53952) iii) TET (adi2mcaRNA27872_R0), iv) MBD2 and MBD (both g53132), v) UHRF1 (adi2mcaRNA19502_R1) and vi) BRG1 (g68733). Points and error bars display mean±standard error of the mean value of the VST normalized data. Red and blue arrows indicate transitions with significant (padj<0.05, log2FoldChange>|1|) down- and up-regulation, respectively.

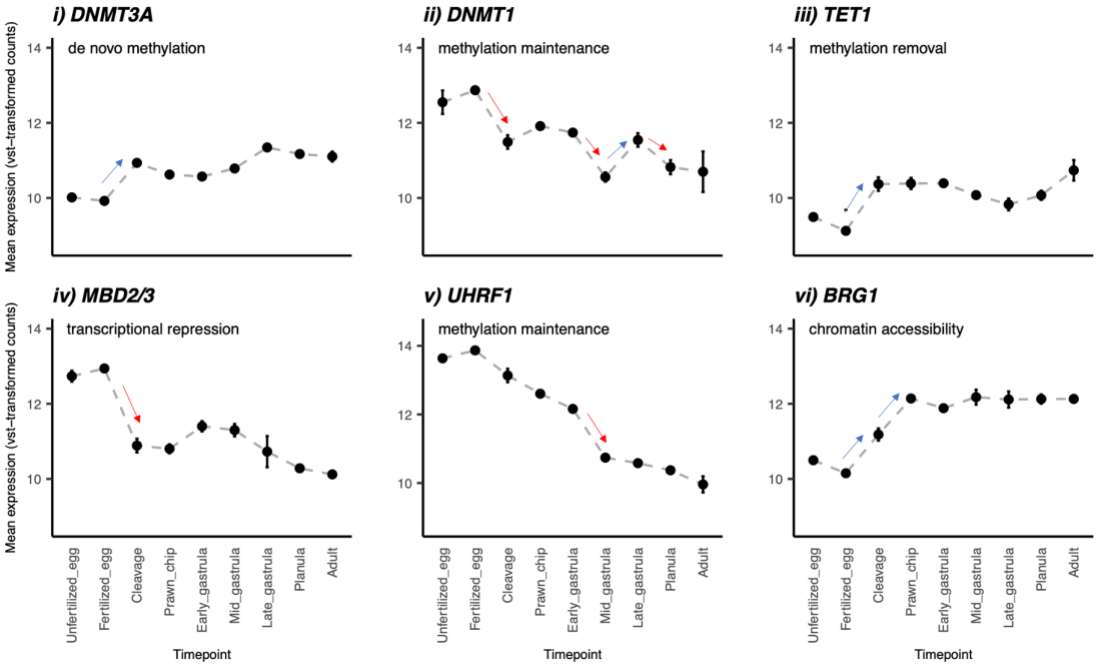

MANUSCRIPT 2

In preparation for *Proceedings of the Royal Society B*.

Development in corals with vertically-transmitted symbionts is resistant to ocean acidification

Chille E [1], Strand E [1], Scucchia F [2], Neder M [2], Schmidt V [3], Sherman M [1], Mass T [2], Putnam HM [1]

Affiliations:
[1] Department of Biology, University of Rhode Island, Rhode Island, USA
[2] Department of Marine Biology, The Leon H. Charney School of Marine Sciences, University of Haifa, Haifa, Israel
[3] Yale School of Medicine, Yale University, Connecticut, USA

Keywords: DESeq2, MZT, maternal provisioning, RNAseq

***Corresponding author:** echille124@gmail.com

Abstract
Reef building corals are under threat from multiple stressors at the local and global scales. Mass mortality has occurred in recent years due to a series of marine heatwaves. In addition, there is chronic stress occurring in the form of ocean acidification, or the decline in pH in surface waters due to the uptake of atmospheric carbon dioxide of anthropogenic origin. In light of these threats to reefs, it is critical to understand coral reproduction and development, which are essential for reef persistence and replenishment in the face of coral loss under climate change. Here we quantify gene expression sensitivity to ocean acidification across a set of developmental stages in the rice coral, *Montipora capitata*. Developing embryos were exposed to three pH treatments ranging from 7.8 (Ambient), 7.6 (Low) and 7.3 (Xlow) from fertilization to 9 days post-fertilization. Embryo and planula volume and gene expression were compared between treatments at each developmental stage to determine the effects of acidified seawater on early development. While there was no measurable size differentiation between fertilized eggs and the prawn chip stage (9 hpf) exposed to ambient, low, and extreme low pH, early gastrula and planula raised in low and extreme low pH treatments were significantly smaller than those raised in ambient seawater, suggesting an energetic cost to developing under low pH. However, no differentially expressed genes emerged between treatments at any time point, except swimming larvae (9 dpf). In a global analysis, principal components analysis shows stronger variation due to life stage, with PC1 showing separation of the life stages and representing 83% of the variance in expression. This suggests that either ocean acidification is not very stressful to organisms not actively calcifying, or that the maternal-to-zygotic transition is robust to pH stress. Planula, however, showed a strong response to reduced pH. Notably, larvae developing at pH 7.8 (Ambient) and pH 7.3 (Xlow) were more similar than those developing at pH 7.6 (Low), which may be due to high CO_2 stimulation of symbiont function at pH 7.3. There was not enough expression data available from the symbiont to test this hypothesis here. Larvae from pH 7.6 showed upregulation of genes involved in cell division, regulation of transcription, lipid metabolism, and oxidative stress in comparison to the other two treatments, supported by smallest sizes in this treatment. While low pH appears to increase energetic demands and trigger oxidative stress, the developmental process is robust to this at a molecular level. Identifying the genes, pathways, and functions underlying the response capacity of embryonic and larval corals to future conditions such as ocean acidification is critical to forecasting coral population resistance and resilience to disturbance.

Introduction

As anthropogenic carbon dioxide (CO_2) levels continue to rise and contribute to global climate change [1], approximately one-third of atmospheric CO_2 is also being absorbed by the surface ocean [2]. Increasing concentrations of CO_2 in the surface ocean leads

to ocean acidification (OA) through a shift in the chemical equilibrium of carbon in seawater [2], thereby reducing ocean pH and lowering the availability of carbonate ions [3]. The absorption of atmospheric CO_2 by the surface ocean has already driven a 0.1 unit decrease in oceanic pH, which is projected to decrease by an additional 0.036–0.042 or 0.287–0.29 units by the year 2100 under best (RCP 2.6) and worst-case (RCP 8.5) scenarios, respectively [1].

A growing body of studies has reported negative effects of reduced seawater pH on marine organisms. OA can negatively impact functionality of marine organisms, in particular biomineralizers that build $CaCO_3$ shells and skeletons [4,5]. Coral reefs are one marine system threatened by OA as reef corals are ecosystem engineers, building skeletons that generate the 3-dimensional complexity and thus habitat for an entire ecosystem. Corals are also threatened by a variety of additional anthropogenic stressors such as marine heatwaves, pollution, sedimentation, and disease [6–8]. While adult organism calcification has been the primary response challenged by OA, less is known about the impact of OA on early life history stages, despite concerns that sensitivity to environmental stressors during early development can present a bottleneck for species persistence in a changing ocean [9,10]. These early life stages are crucial for the resilience of species given their role in repopulating and replenishing existing populations [11,12].

OA can affect multiple early developmental processes in corals and other marine invertebrates. Specifically, under lower pH there are impacts on sperm motility [13–15], fertilization success [9,13,15–19], larval settlement [13,16,20], and post-

settlement growth [16,20,21]. In corals, decreased fertilization efficiency has been observed, which may be explained by decreased sperm flagellar motility and increased polyspermy under low pH [16,17]. Low pH is also correlated with metabolic depression in many coral species [22–25], which may explain observations of delayed development, smaller embryo/larval volume, and reduced post-settlement growth in corals developing in acidified conditions [20,23,26,27]. The increased energetic costs of maintaining homeostatic processes under disrupted acid-base balances and ionic gradients can additionally slow development and reduce growth during early development [20,28]. Similar patterns have been seen in other marine invertebrates as well [9,10]. For example, low pH is correlated to delayed cleavage [29], smaller larvae [30], and depressed metabolism [31] during the early development of sea urchins. Developmental delays [28,32] and decreases in fertilization rate [33–35], hatching success [35–37], larval survival [35,37] and larval size, [32,35,37] have also been observed in bivalves under low pH. These compounding effects of low pH drastically decrease successful coral recruitment [13,16], eliciting concerns on downstream effects on coral reef resilience [11,12].

Most studies examining the effects of OA on coral development thus far have focused primarily on fertilization, settlement, and post-settlement growth, with less of a focus on embryonic development. In many species, embryogenesis represents a critical window in development during which time embryos are particularly sensitive to environmental fluctuations outside of the expected range [9,10,29,38–41]. Several studies have implicated the loss of maternal defenses during the maternal-to-zygotic transition (MZT) in increased environmental sensitivity during this period [10,29,40–

42]. The MZT describes the developmental reprogramming of gene expression from maternal to zygotic regulation [43,44]. During the MZT, the maternally-provided gene products that regulate early development and protect embryos from expected stressors are degraded as zygotic transcription activates and intensifies [43,44]. Higher mortality in response to environmental perturbations has been observed during this transition in fish gastrula [41,42], sea urchin blastula/gastrula [29,40], and several other marine invertebrates [10].

Maternal mRNA provisioning and the timing of the MZT in reef-building corals, thus far, have only been investigated in the Hawaiian rice coral, *Montipora capitata*. Under ambient conditions, the maternal mRNA complement in *M. capitata* eggs primarily provide housekeeping functions, including cell cycle, biosynthesis, transcription, signaling, and protein processing [45,46]. However, DNA repair mechanisms, which may protect early embryos from UV radiation and reactive oxygen species (ROS), are also over-represented in the *M. capitata* maternal mRNA complement of eggs [45]. In the previous studies, un-adenylated maternal mRNAs that provide additional stress-response functions may not have been captured because they may only be adenylated (activated) under stressful conditions. As of yet, the maternal mRNA complement in reef-building corals has not been assessed under stressful conditions. However, based on timing of the MZT in *M. capitata* [45], and developmental gene expression studies in *Acropora millepora* [47], *Acropora digitifera* [48], and *Nematostella vectensis* [49], coral embryos may be most sensitive to stress during early gastrulation (between 9 and 14 hours post-fertilization (hpf)), when a large portion of maternal transcripts are degraded and zygotic transcription begins.

Previous transcriptomic examinations of pH-stress during coral development have been done on aposymbiotic species (Acropora [47] and on post-settlement stages after the completion of the MZT (Moya et al., 2012). Here, we use *Montipora capitata*, a hermaphroditic broadcast spawner with vertical symbiont transmission that is endemic to the Hawaiian archipelago [50,51] to examine the embryonic sensitivity to OA in the context of the MZT. In this study, we examined the physiological and transcriptomic outcomes of early coral development in five life stages from fertilization until the "completion" of early coral development (i.e. fully-developed larvae) under pH 7.8 (ambient), and two low pH conditions (7.6 and 7.3). This time series allows us to determine sensitivity to and phenotypic consequences of OA during and after the MZT.

Methods

Specimen collection

Montipora capitata egg-sperm bundles were collected under the Department of Land & Natural Resources Special Activity Permit 2018-50 from the reef adjacent to the Hawai'i Institute of Marine Biology (HIMB), Coconut Island, Kāne'ohe Bay, O'ahu Hawai'i (21°25'58.0"N 157°47'24.9"W) at ~21:00 on June 13, 2018. After collection, egg-sperm bundles were allowed to break apart. Eggs were separated from the sperm and rinsed 3 times with 0.2 uM filtered seawater, then snap-frozen and stored at -80 °C in ~300 uL aliquots.

Experimental set-up

Fertilization and early development occurred in nine 1.6 L conicals flow-through tanks set to pH 7.8 (ambient), pH 7.6, and pH 7.3 pH (n=3 conical tanks per treatment, Fig1A). At 22 hpf, the embryos were transferred to replicate 118 ml bins with 152µm plankton mesh bottoms floating in 74L glass tanks (n=3 bins per tank, 2 tanks per treatment; Fig. 1A) Treatments were designed to reflect future ocean acidification conditions in coastal embayments [52,53] including daily fluctuations naturally occurring in Kāneʻohe Bay, Hawaiʻi [54]. All treatments were controlled by a pH-stat feedback system in one header tank per treatment. Header tank conditions were continuously monitored using a Neptune Apex Reef Aquarium set-up (Energy Bar 832; Controller Base Unit; PM1 pH/ORP Probe Module; Extended Life Temperature Probe; pH Probe), and 99.99% food-grade CO_2 was injected into the header tanks with gas flow solenoids (Milwaukee MA955) using inline venturi injectors (Forfuture-go G1/2 Garden Irrigation Device Venturi Fertilizer Injector) in a pressure driven line connected to a circulating pump (Pondmaster Pond-mag Magnetic Drive Water Pump Model 5) in each header tank (Fig. 1A). Water flow was delivered at a maximum potential flow rate of 7.57 liters per hour by 1.9 LPH (½ GPH) Pressure Compensating Drippers for a conical turnover rate of once every ~50 minutes, and once every ~23 hours for a 74 L tank. The average light intensity, 96±8.823 mean±sem umol m^{-2} s^{-1}, was measured using a handheld PAR sensor (Underwater Quantum Flux Apogee instruments - Model MQ-510; accuracy = ±4%).

Temperature, salinity, and pH were measured three times daily in each treatment tank using a handheld digital thermometer (Fisherbrand Traceable Platinum Ultra-Accurate Digital Thermometer, accuracy = ±0.05 °C, resolution = 0.001°) and a portable

multiparameter meter (Thermo Scientific Orion Star A series A325; accuracy = ±0.2 mV, 0.5% of psu reading, resolution = 0.1 mV, 0.01 psu) with pH and conductivity probes (Mettler Toledo InLab Expert Pro pH probe #51343101; Orion DuraProbe 4-Electrode Conductivity Cell Model 013010MD), respectively (Table 1). Temperature and pH probes were calibrated using Tris (Dickson Laboratory Tris Batch 27, Bottles 70, 75, 167, 245, and 277) standard calibrations. Total alkalinity (µmol kg^{-1} seawater) was measured from water samples daily using an automated titrator (Mettler Toledo T50) and hydrochloric acid (Dickson Laboratory Titrant A3), and certified reference material (Dickson Laboratory CO_2 CRM Batch 149) was used as a quality control standard. Carbonate chemistry parameters (pH, CO_2, pCO_2, HCO_3, CO_3, dissolved inorganic carbon, total alkalinity, and aragonite saturation) were calculated from total alkalinity measurements using SEACARB v3.0.11 [55] in RStudio (Table 1 and Table S1) using Kf from [56], K1 and K2 from [57] and Ks from [58]. Seawater pH was calculated on the total scale [59]; SOP6a), using the gas constant (8.31447215 J K^{-1} mol^{-1}) and the Faraday constant 96485.339924 coulombs mol^{-1}).

Sample collection and preservation

Physiological and molecular samples were taken immediately upon egg-sperm bundle collection and at seven timepoints following transfer to experimental conditions (Fig. 1B). Sampling times represent visually-distinct developmental stages including fertilized embryo (1-hr post-fertilization), cleavage (4-hr post-fertilization), prawn chip (9-hr post-fertilization), early gastrulation (14-hr post-fertilization), and planula (9-d post-fertilization). Physiological samples (~100-200 embryos or larvae per replicate) were preserved in 500 µL 25% zinc buffered formalin in 0.2µm filtered

seawater, and stored at 4°C. Molecular samples (300 µL of embryos per replicate) were snap-frozen in liquid nitrogen and stored at -80°C.

Embryo development and growth

Stereomicroscope images of fixed samples were analyzed for blastomere number at 4 hpf (cleavage stage), and for maximum length and perpendicular width of the unfertilized eggs, gastrula, and planula using ImageJ. Cell division stage was assessed in cleavage-stage samples with 82 to 282 embryos/sample (n=3 replicate treatment^{-1}). Embryos were classified as "one cell," "two cells," "four cells," or "greater than four cells." The percentage of embryos at each stage of cell division was then calculated for each sample to examine potential variation in developmental timing between treatments. Volume of unfertilized eggs (n=50), fertilized embryos (n=225), early gastrula (n=200), and planulae (n=150) was calculated using the equation for an oblate ellipse: V=43ab2in which Vis equal to volume, a is the half of maximum width and b is the half maximum length to examine differences in size between treatments through early development.

All statistical analyses for morphological data were performed in RStudio (v1.3.959; [60], using R version 4.0.2 [61]. A beta regression model was used to analyze variation in the proportion of cells at each cleavage stage and treatment. Additionally, a one-way nested ANOVA analysis tested the effect of tank on embryo and planula size wherein tank ID was nested within treatment. After determining that tank effects were insignificant ($P > 0.05$), one-way ANOVA analysis was used to test for the effect of treatment on fertilized embryo, gastrula, and planula volume. Post hoc Tukey

HSD tests were conducted when the effect of treatment was significant ($P < 0.05$). Data were visually examined for normal distribution and equal variance. The dependent variable was square-root transformed for the gastrulation and planula life stages in order to meet statistical assumptions prior to ANOVA analysis. Data points for these life stages were back-transformed for visualization in Figure 2.

RNA extraction, sequencing, and processing

To extract RNA, molecular samples were digested at 55°C in 300 µl of DNA/RNA Shield (Zymo Research, Irvine, CA, USA) for two to three-and-a-half hours and centrifuged at 2200 RCF for one minute to separate the remaining solids. Total RNA was extracted from each supernatant with the Zymo Quick-DNA/RNA™ Miniprep Plus Kit (Zymo Research, Irvine, CA, USA) following the manufacturer's protocol for tissue samples. RNA was quantified (ng/µL) with a ThermoFisher Qubit Fluorometer and quality was assessed using the Eukaryote RNA analysis on the Agilent TapeStation 4200 System. Total RNA samples were then sent to Genewiz (South Plainfield, New Jersey, USA) for library preparation and sequencing. cDNA libraries were constructed following the TruSeq Stranded mRNA Sample Preparation protocol (Illumina, San Diego, CA, USA) and sequenced on a HiSeq instrument targeting 15 million reads per sample. Quality trimming, alignment, and assembly were conducted as described in [45]. In short, sequences were filtered for quality applying a five base pair sliding window to remove reads with an average quality score less than 20, and retaining sequences with quality scores greater than or equal to 20 in at least 90% of bases and sequence length greater than or equal to 100 bases. Trimmed reads were then aligned to an *M. capitata* reference assembly [62] using HISAT2 in the stranded

paired-end mode [63], and assembled with StringTie in the stranded setting (v2.1) [64]. Finally, the StringTie *prepDE* python script [64] was used to generate a gene count matrix from the resulting GFFs [64].

Global gene expression analyses

Experiment-wide patterns in gene expression were assessed with a principal coordinates analysis (PCA). First, the full gene count matrix was pre-filtered to reduce the memory size dataframe, increase the speed of processing, and improve quality of statistical analysis by removing low-coverage counts. As such, filtering was carried out with the Genefilter (v1.70.0; [65]) function *pOverA* to exclude genes where fewer than 2 out of 41 (~0.0488) samples had counts under 10. Then, counts were transformed with DESeq2's (v1.28.1) variance stabilizing transformation function (vst) [66] after confirming that all size factors were less than 4. Finally, the vst-transformed counts were used for PCA to visualize expression results for all filtered genes. The DESeq2 *plotPCA* function was used to generate a PCA of all samples based on sample-to-sample distance. All gene expression analyses were performed in RStudio (v1.3.959) [60], using R version 4.0.2 [61].

Differential gene expression analysis

PCA and differential gene expression analysis with DESeq2 were used to assess within-stage differences in expression due to treatment. As described above, genes with low overall expression were filtered using the Genefilter *pOverA* filter function [65]. After testing a range of values from p=0.33 to p=0.9, a more conservative value of p=0.875 was chosen to prevent bias due to high duplication levels in the first four

life stages where zeros likely represent true zeros compared to the planula samples which had lower duplication. As such, we retained genes with greater than 10 counts in at least 7 out of 8 samples (pOverA 0.875, 10) for further analysis. The resulting genes were then vst-transformed using the DESeq2 *vst-transformation* function [67]. PCA was conducted with the DESeq2 *plotPCA* function [67], using vst-transformed counts to calculate sample-to-sample distance. Differential expression analysis between pH treatments was then performed for each life stage using the filtered counts (pOverA 0.875, 10). Pairwise differences in gene expression between treatments were estimated using Wald model in DESeq2 (Love et al., 2014). As DESeq2 results showed zero differentially-expressed genes (DEGs) in all treatment comparisons prior to the planula stage, only genes with padj<0.05 in the planula stage were used for further analysis. To visualize the DEGs that were shared and distinct for each treatment comparison within the planula stage, the results were summarised as a venn diagram (Fig. 4A) using the VennDiagram R package v1.6.20 [68]. Overall expression patterns among the planula DEG set were visualized as a heatmap using the ComplexHeatmap package v2.5.4 [69], with clustering based on differences in expression compared to the rowmean in the vst-transformed count matrix. Clusters in the heatmap are based on k-means clustering using the R package NbClust v3.0 [70] to calculate the optimal number of clusters using 30 indices.

Gene ontology enrichment analysis

Gene ontology (GO) enrichment analysis was performed on the planula DEG set to examine the biological processes and molecular functions primarily correlated with each DEG k-means cluster. GO enrichment analysis was performed on the DEGs with

log2FoldChange > 2 in each k-means cluster using the R package Goseq (v1.40.0) [71], using the functional annotation of the *M. capitata* genome from [45] as input for the GOseq category test. Subsequently, slim categories for the enriched terms were obtained using the *goSlim* function in the R package, GSEABase, using the generic GOslim obo database as reference (http://current.geneontology.org/ontology/subsets/goslim_generic.obo; v1.2) [72]. Redundant slim categories were removed, keeping the parent slim function. Finally, enriched biological process and molecular function terms with numInCat > 5 and their associated slim categories were visualized as a heatmap using the ggplot2 *geom_tile* function [73].

Symbiont transcriptome assembly and gene expression analysis

To assess correlation between pH Treatment and gene expression of Symbiodinaceae within the planula host, the symbiont transcriptomes were extracted from a *de novo*-assembled holobiont sequence library and analysed for differential expression between treatments. The holobiont transcriptome was assembled *de novo* using Trinity v2.12.0 [74] with the stranded 'RF' option. All cleaned planula fastq files were used to assemble the holobiont transcriptome. In addition, cleaned fastq files corresponding to three adult *Montipora capitata* samples from [45], prepared using the pipeline described above, were also used to construct the holobiont transcriptome in order to obtain a symbiont-rich library. Following assembly, completeness was assessed using BUSCO v4.0.6 [75] to detect the presence of single-copy orthologs universal to alveolata (for the symbionts) and metazoans (for the host). The host and symbiont transcriptomes were then extracted from the holobiont assembly using *psyTrans*

(https://github.com/sylvainforet/psytrans) using *Cladocopium* C1 [76,77] and *Montipora capitata* [62] predicted proteins as references. Following separation, the symbiont reads were used as a reference file for the Trinity *align_assemble* perl script [74] using RSEM v1.3.3 [78] for abundance estimation and Bowtie v-1.2.1.1 as the alignment method [79]. Accordingly, the host sequences were also aligned and assembled with Trinity to provide a comparison for quality assessment of the symbiont extraction and assembly. Finally, the symbiont gene counts were obtained using the Trinity *abundance_estimates_to_matrix* perl script [74]. Differential gene expression of the planula endosymbionts was carried out using the methods described for the host early life stages (see *Differential gene expression analysis*). Finally, the identities of the symbiont DEGs were determined through a local alignment search of the corresponding sequences against the NCBI non-redundant database using Blastx v2.11.0 [80] with default parameters.

All raw data can be accessed on the NCBI SRA repository under the Bioproject accession IDs, PRJNA731596 (adult) and PRJNA616341 (all other timepoints). Additionally, all scripts used for bioinformatic and statistical analyses are available on the GitHub repository, Mcapitata_OA_Developmental_Gene_Expression_Timeseries.

Results

Embryo development and growth

Immediately after release, prior to treatment exposure, eggs were 0.040±0.023 mm^3 (Fig. 2A). Following treatment exposure, the proportion of embryos at each cleavage stage at 4hpf and embryo size in the fertilized egg (1hpf), early gastrula (14hpf), and

planula (9dpf) samples was assessed to characterise morphological effects of developing in ambient (7.8) low (7.6) and extreme low pH (7.3) conditions. At the cleavage stage, across all treatments combined undivided cells were on average more frequent (44.77 ± 21.49%; mean ± sd) than those at the two-cell (26.51 ± 12.63%), four-cell (18.37 ± 11.23%), or greater-than-four cell stage (10.34 ± 13.40%). Beta regression analysis of the proportion of cells at each cleavage stage and treatment (Fig. 2B) shows that while there were significant differences (<0.0001) in proportions of two-, four-, and greater-than-four cell stages overall, the interaction between cleavage stage and treatment were only marginally significant (p=0.0765). Additionally, there were no significant differences between pH treatments in embryo size in the fertilized eggs (p=0.256; Fig. 2C). However, at both the early gastrula (p=0.000292; Fig. 2D) and planula stages (p=0.000109; Fig. 2E) embryos developing under ambient pH conditions were significantly larger than those developing under the low and extreme low conditions.

RNA sequencing, quality control, and mapping

TruSeq Illumina Stranded Paired-End (PE) sequencing resulted in 935,000,000 PE (19,392,156 mean reads/sample), with 694,800,000 PE reads (14,241,176 mean reads/sample) remaining after quality filtering and adapter removal. On average, 79.28 ± 1.95% mean ± sem reads per sample aligned to the reference *M. capitata* genome [62]. Assembly quality assessment with GFFcompare showed that 63,227 genes queried from the mapped GTF files were matched to the 63,227 genes in the reference genome [62], with 40,883 matching intron chains, 63,218 matching loci, and zero missing elements.

Global gene expression patterns

After filtering to remove genes with fewer than 10 counts in ~4.88% of samples (i.e., the proportion representing each treatment in a given life stage), 30,271 genes remained to characterize global gene expression patterns. A principal components analysis (Fig. 3A) shows that sample-to-sample variation is primarily related to differences in life stage, with PC1 (83%) and PC2 (12%) explaining the majority of variation between life stages.

Differential gene expression

Principal components analyses computed from variation in expression of genes with greater than ten counts in seven of eight fertilized egg (10,751 genes; Fig. S1A), cleavage (12,837 genes; Fig. S1B), prawn chip (16,392 genes; Fig. S1C), early gastrula (17,669 genes; Fig. S1D), and planula (23,225 genes) samples show no differentiation between treatments until the planula stage (Fig. 3B). At the planula stage, treatment groups separate strongly along PC1 and PC2, which explain 47% and 25% of the variation between samples, respectively. Notably, ambient pH (7.8) and extreme low pH (7.3) samples cluster closer than ambient and low pH (7.6) samples on PC1. However, with the exception of one ambient sample, ambient and low pH samples cluster closer than ambient and extreme low pH samples on PC2 (Fig. 3B).

Pairwise treatment comparisons within each life stage using DESeq2 (Table S2) showed zero differentially expressed genes between treatments until the planula stage. Differentiation of samples from planula raised in different treatments along PC1 and PC2 of in the planula PCA (Fig. 3B) is primarily explained by 5,406 DEGs between

planula samples raised under the two low pH conditions relative to the ambient pH conditions. Mirroring the clustering of treatments along PC1 in Fig. 3B, a venn diagram (Fig. 4A) of shared and unique DEGs in each treatment comparison shows 2,202 DEGs between planula the low and ambient pH treatments, 1,078 of which are also differentially expressed between the extreme low and low treatments. Only 66 DEGs exist between planula the extreme low and ambient pH treatments. Planula DEGs were grouped into two k-means clusters based on the consensus of 11 of 30 clustering indices (Fig. 4B), with genes in Cluster 1 upregulated in the low pH treatment compared to the ambient and extreme low pH treatments, and genes in Cluster 2 exhibiting the opposite pattern (Fig. 4B).

Gene ontology enrichment

After filtering the DEG set to retain genes with log2FoldChange>|1|, 344 DEGs remained in Cluster 1 (upregulated under low pH), and 256 remained in Cluster 2 (downregulated under low pH) for GO enrichment analysis. GO enrichment analysis revealed 39 biological processes and 31 molecular functions over-represented in Cluster 1. Biological processes overrepresented in Cluster 1 (Fig. 5A, Table S3) are primarily related to 7 slim terms, including biosynthetic process, cellular component assembly, cellular nitrogen compound metabolic process, immune system process, lipid metabolic process, response to stress, and transport. Likewise, molecular functions overrepresented in Cluster 1 (Fig. 5B, Table S3) can be summarised by 8 slim terms, including ATPase activity, cytoskeletal protein binding, DNA binding, ion binding, kinase active, oxidoreductase activity, structural molecule activity, and transferase activity. In Cluster 2, GO enrichment revealed 5 overrepresented biological

processes (Fig. 5A, Table S3) represented by the slim terms biosynthetic process, immune system process, and transport, as well as 10 overrepresented molecular functions (Fig. 5B, Table S3) represented by the slim terms, ATPase activity, nucleotidyltransferase activity, peptidase activity and transmembrane transporter activity.

Symbiont transcriptome assembly and gene expression analysis

The *M. capitata* planula and adult holobiont assembly was constructed from 698,861,565 bases, yielding 991,330 transcripts and 656,603 genes. The N50 of the holobiont assembly was 1,102, with an average contig length of 704.97 bases and a GC content of 43.7%. A BUSCO search of the holobiont assembly against the metazoan and alveolata databases for the host and symbiont showed high completeness (90.1% alveolata and 97.5% metazoan). In total, 83.37% (826,513) of transcripts from the holobiont assembly were assigned to the host and 16.63% (164,817) of transcripts were assigned to the symbiont. Finally, using the separated assemblies as reference transcriptomes for Trinity, 4.77±0.43% (mean±se) of planula sequences aligned to the symbiont, yielding 133,811 symbiont genes for differential expression analysis. Additionally, 88.34±0.40% of sequences aligned to the host with Trinity, which is slightly lower than the planula alignment rate to the *M. capitata* genome using HISAT2 (91.09±0.35%).

After filtering to remove reads with fewer than 10 counts in 7 out of 8 samples, 1,365 genes remained for principle components and differential expression analyses. A principle components analysis (Fig. S2A) of the symbiont samples shows large

variation in gene expression between the three low pH (7.6) samples along the PC1 (28%) and PC2 (14%) axes, but the samples from the ambient pH (7.8) and extreme low pH (7.3) each cluster by treatment. Differential gene expression analysis with DESeq2 (Table S4) revealed 12 differentially-expressed genes (DEGs) between the ambient and low treatments, 17 DEGs between the ambient and extreme low treatments, and 0 DEGs between the low and extreme low treatments. The ten symbiont genes upregulated in the low treatment compared to the ambient aligned to the histone H3 protein as well as actin and tubulin proteins, while the two downregulated genes aligned to the pre-mRNA-splicing factor ATP-dependent RNA helicase and a cell wall-associated hydrolase (Table S5). However, the seventeen symbiont genes upregulated in extreme low treatment (Table S5) compared to the ambient were primarily associated genes regulating rDNA expression, a mucin-like protein, cytochrome P450, COPB protein, as well as several hypothetical proteins.

Discussion

Limited research has been conducted so far on the effects of OA on coral embryonic development, with a primary focus on physiological processes [81,82], while little is known about the changes occurring at the transcriptomic level. Here we show that while acidic seawater altered the morphological development of *M. capitata* embryos, it did not drive any substantial change in gene expression until after the MZT. Early gastrula and planula developing at pH 7.6 (low) and pH 7.3 (extreme low) were significantly smaller than those developing at pH 7.8 (ambient), suggesting an energetic cost to developing under low pH. This is also supported by functional enrichment of the genes associated with cell division, regulation of transcription, lipid

metabolism, and oxidative stress that are significantly upregulated in swimming larvae (9 dpf) exposed to pH 7.6. We additionally show that transcriptomically, larvae developing at pH 7.8 and pH 7.3 were more similar than those developing at pH 7.6 and hypothesize that this may be due to high CO_2 stimulation of symbiont photosynthesis at pH 7.3.

The MZT under ocean acidification

While the morphological effects of low pH were apparent by the early gastrula stage (22 hpf; Fig. 2D-E), pH did not drive any substantial changes in gene expression until the larval stage, i.e., after the zygotic transcriptome has assumed autonomy [45] (Fig. S1). These results suggest that the maternal-to-zygotic transition in *M. capitata* is robust to low pH. While this study lacks support from survivorship data, this finding is supported by other studies on OA stress during the embryonic development of fish [41,42] and sea urchins [29,40] that show that while early development is robust to ocean acidification, embryos are more vulnerable after the MZT. These findings support the role of maternal gene products (i.e., mRNA, proteins, transcription factors) in buffering early embryos from environmental stress. In *M. capitata*, early development is likely to be influenced by maternal transcripts until 22-36 hpf, when the zygotic transcriptome exhibits the capacity for responding to stimuli [45]. Seeing as a transcriptomic response to decreased pH was only apparent at the planula stage (Fig. 3b & Fig. 4), this suggests that the transcripts necessary to buffer embryonic development from OA are already expressed under ambient conditions or that embryos possess other molecular defenses, such as maternally-provisioned proteins [83] that buffer the effects of low pH. However, maintaining homeostasis under low

pH comes with an energetic cost, as indicated by the smaller sizes of embryos developing low pH. As such, while the embryonic development of *M. capitata* may be robust to ocean acidification, the energetic cost of developing low pH may have latent effects on larval competence and recruitment [13].

Outcomes of developing in low pH

In our study, low pH (pH 7.6) elicited a robust transcriptomic response in planula that implicates several processes affecting energy metabolism and larval size (Fig. 2E), including biomineralization, cellular acidosis, and cellular stress response. We detail these responses below.

Several studies have found that actively calcifying larvae may be more susceptible to changes in seawater carbonate chemistry compared to non-calcifying embryos and larvae [9,10] by making biomineralization more chemically and energetically difficult [84]. In corals, calcium carbonate deposition is initiated during the pre-settled larval phase [85]. While mineralization was not specifically examined, as nine-day-old larvae, it is likely that the planula here were at the calcifying stage. In fact, gene ontology enrichment analysis shows that genes associated with calcium ion binding and calcification, including the CUB domain (adi2mcaRNA18251_R0), cadherin (adi2mcaRNA22715_R0, g25241), the EF-hand calcium-binding motif (g14107, g21537, g62869), calmodulin (g44605), and calreticulin (g59987) are upregulated in larvae exposed to pH 7.6 (Table S3). These genes provide structural and cell adhesion functions that aid in the biomineralization process [86] and may be upregulated to compensate for the chemical shift in carbon equilibrium in the seawater [87–89].

However, upregulation of these genes in response to OA may increase energetic demand, as observed in some adult corals [90,91]. This increased demand could potentiate the rapid depletion of larval lipid stores if the energy derived from their endosymbionts is insufficient to keep up with demand [92–94], ultimately decreasing larval size.

Acid-base parameters such as pH and pCO2 are generally considered to lead to depressed metabolism through cellular acidosis, leading to alterations in cell size [95,96]. Here, the enrichment of terms related to ATP synthesis (e.g., ATP synthesis coupled proton transport [GO:0015986], ATPase activity [GO:0016887]) in the genes downregulated at low pH (pH 7.6; Table S3), and lipid metabolism (e.g., phospholipid metabolic process [GO:0006644], phospholipid catabolic process [GO:0009395]) in the genes upregulated at low pH (pH 7.6; Table S3) suggests alteration of larval metabolism at reduced pH. Metabolism is highly interconnected with both growth and cell cycle progression [97]. Additionally, mitochondria play a crucial role in setting growth rates through energy generation and lipid biosynthesis [98]. In this context, alteration in metabolism at low pH might cause changes in cell size. Here, the enrichment of terms related to cell growth and cytoskeleton (e.g., cell cycle [GO:0007049], cellular component assembly [GO:0022607], cytoskeleton organization [GO:0007010]) in the genes upregulated at low pH 7.6 (pH 7.6; Table S3) suggests changes in cell cycle and cell size with acidification. Cell growth-related genes such as JNK cascade and GTPase activity have been shown to change with acidification [99], and acidic cellular pH was demonstrated to alter processes such as

cytoskeletal integrity [100]. Such alterations in cytoskeletal integrity could explain the observed smaller size of planula that developed under reduced pH conditions.

Chronic exposure to low pH (pH 7.6) during early development also appears to elicit the onset cellular stress and antioxidant responses. Planula developing at pH 7.6 showed functional enrichment of the GO terms "response to oxidative stress [GO:0006979]", "immune response [GO:0006955]", "superoxide metabolic process [GO:0006801]", "oxidation-reduction process [GO:0055114]", and "microtubule-based process [GO:0007017]" (Table S3). These GO terms are linked to protein domains that protect the cell from oxidative stress through oxidoreductase activity (e.g., superoxide dismutase-like [101–104], peroxidasin-like [96,101], FAD-linked oxidase [96,105–107]) and removal of damaged cells (e.g., Toll/interleukin-1 receptor [108–110], TNF receptor-associated factor 4 [111,112]). Upregulation of cellular stress and antioxidant responses is consistent with stress response mechanisms documented in adult and larval corals upon exposure to multiple stressors, including low pH [96], ultraviolet radiation [106], and thermal [105,107,113,114], and nutrient stress [113]. Here, cellular stress and antioxidant responses may have been induced from macromolecular damage due to ROS released from the rapid peroxidation of planula lipid stores for energy use [114] or from increased ROS production by the algal endosymbiont. Notably, however, the onset of cellular stress response may also come at an energetic cost to the planula [115] and lead to smaller larvae by depleting maternal lipid stores.

Symbiont stimulation under high CO_2

Predicted future increase of CO_2 in seawater has been shown to stimulate the photosynthetic activity of the algal symbiont [116,117]. Such stimulation enhances the host fitness under acidification [118]. In this study, the enrichment of terms related to coral oxidative stress under pH 7.6 (low; Table S3) suggests increased photosynthetic activity in the endosymbiotic algae due to the higher availability of CO_2 in seawater, as observed in the endosymbionts of *Stylophora pistillata* primary polyps [119]. It has been hypothesized that at higher concentrations of CO_2 the stimulation of symbiont photosynthesis could prevent acidosis of the host cells, thus helping with preserving cellular acid-base homeostasis [120], and ultimately alleviating the effects of OA on the host fitness, as observed here in planula developing at pH 7.3 (Xlow). However, our symbiont gene expression data do not support this hypothesis. Of the 29 genes differentially expressed in the low pH treatments (pH 7.6 and pH 7.3; Table S4) compared to the control (7.3), the majority encoded enzymes that provide housekeeping functions, such as tubulin, rRNA promoter binding proteins, and rDNA transcriptional regulator 15 (Table S5). We hypothesize that the differential expression of these few genes may be related to library size and that there is not enough expression coverage in the dataset to have the power to test our hypothesis for the symbionts.

Conclusions

In this study, we examined developmental sensitivity to and phenotypic consequences of OA during and after the MZT in the rice coral, *Montipora capitata*. While on a transcriptomic level, no differential gene expression was observed until after the MZT,

phenotypically, early gastrula (14 hpf) and fully-developed larvae developing in the pH 7.6 (low) and pH 7.3 (Xlow) treatments were significantly smaller than those in the control (pH 7.8). This supports that the development of *M. capitata* embryos is resilient to low pH conditions, even those substantially lower than what currently occurs in Kāneʻohe Bay. While the MTZ appears to be robust to OA, the energetic strain on larvae from maintaining homeostasis under low pH could create negative carryover effects for the energetically costly process of metamorphosis [121] as well as energetic challenges associated with competition and predation effects on coral early life stages. Lowered fitness in these early life stages could potentially create an ontogenetic bottleneck that impacts the repopulation and replenishment of coral reefs and contribute to their continued decline [122]. Of note, however, the reductions in body size detected so far in coral larvae represent the effects of future OA conditions on modern populations, without considering any potential moderating effects of rapid adaptation or acclimatization, which is pivotal to accurately forecast the impacts of climate change on marine organisms [30,123].

Acknowledgements

We would like to extend our deepest gratitude to the faculty and staff of the Hawaiʻi Institute of Marine Biology and the University of Rhode Island Computing for accommodating us and for their technical support.

Funding

This work was funded by BSF grant 2016321 to HMP and TM. This work was also partially supported by the USDA National Institute of Food and Agriculture, Hatch Formula project accession number 1017848.

References

1. Bindoff NL *et al.* 2019 Changing Ocean, Marine Ecosystems, and Dependent Communities. In (eds H-O Pörtner, DC Roberts, V Masson-Delmotte, P Zhai, M Tignor, E Poloczanska, K Mintenbeck, A Alegría, M Nicolai, A Okem, et al.), pp. 477–587. Switzerland: Intergovernmental Panel on Climate Change.

2. Sabine CL *et al.* 2004 The oceanic sink for anthropogenic CO2. *Science* **305**, 367–371. (doi:10.1126/science.1097403)

3. Caldeira K, Wickett ME. 2003 Oceanography: anthropogenic carbon and ocean pH. *Nature* **425**, 365. (doi:10.1038/425365a)

4. Doney SC, Fabry VJ, Feely RA, Kleypas JA. 2009 Ocean acidification: the other CO2 problem. *Ann. Rev. Mar. Sci.* **1**, 169–192. (doi:10.1146/annurev.marine.010908.163834)

5. Kroeker KJ, Kordas RL, Crim RN, Singh GG. 2010 Meta-analysis reveals negative yet variable effects of ocean acidification on marine organisms. *Ecol. Lett.* **13**, 1419–1434.

6. Hughes TP *et al.* 2017 Coral reefs in the Anthropocene. *Nature* **546**, 82–90. (doi:10.1038/nature22901)

7. Harvell CD, Mitchell CE, Ward JR, Altizer S, Dobson AP, Ostfeld RS, Samuel MD. 2002 Climate warming and disease risks for terrestrial and marine biota. *Science* **296**, 2158–2162. (doi:10.1126/science.1063699)

8. Maynard J *et al.* 2015 Projections of climate conditions that increase coral disease susceptibility and pathogen abundance and virulence. *Nat. Clim. Chang.* **5**, 688–694.

9. Byrne M. 2012 Global change ecotoxicology: Identification of early life history bottlenecks in marine invertebrates, variable species responses and variable experimental approaches. *Mar. Environ. Res.* **76**, 3–15. (doi:10.1016/j.marenvres.2011.10.004)

10. Przeslawski R, Byrne M, Mellin C. 2015 A review and meta-analysis of the effects of multiple abiotic stressors on marine embryos and larvae. *Glob. Chang. Biol.* **21**, 2122–2140. (doi:10.1111/gcb.12833)

11. Adjeroud M, Kayal M, Penin L. 2017 Importance of Recruitment Processes in the Dynamics and Resilience of Coral Reef Assemblages. *Marine Animal Forests*. , 549–569. (doi:10.1007/978-3-319-21012-4_12)

12. Ritson-Williams R, Arnold SN. 2009 New perspectives on ecological mechanisms affecting coral recruitment on reefs. *Contributions to the …*

13. Albright R. 2011 Reviewing the Effects of Ocean Acidification on Sexual Reproduction and Early Life History Stages of Reef-Building Corals. *J. Mar. Biol.* **2011**, 1–14. (doi:10.1155/2011/473615)

14. Morita M, Suwa R, Iguchi A, Nakamura M, Shimada K, Sakai K, Suzuki A. 2010 Ocean acidification reduces sperm flagellar motility in broadcast spawning reef invertebrates. *Zygote* **18**, 103–107. (doi:10.1017/S0967199409990177)

15. Havenhand JN, Buttler F-R, Thorndyke MC, Williamson JE. 2008 Near-future levels of ocean acidification reduce fertilization success in a sea urchin. *Curr. Biol.* **18**, R651–R652. (doi:10.1016/j.cub.2008.06.015)

16. Albright R, Mason B, Miller M, Langdon C. 2010 Ocean acidification compromises recruitment success of the threatened Caribbean coral Acropora palmata. *Proc. Natl. Acad. Sci. U. S. A.* **107**, 20400–20404. (doi:10.1073/pnas.1007273107)

17. Albright R, Mason B. 2013 Projected near-future levels of temperature and pCO2 reduce coral fertilization success. *PLoS One* **8**, e56468. (doi:10.1371/journal.pone.0056468)

18. Han Y, Shi W, Tang Y, Zhao X, Du X, Sun S, Zhou W, Liu G. 2021 Ocean acidification increases polyspermy of a broadcast spawning bivalve species by hampering membrane depolarization and cortical granule exocytosis. *Aquat. Toxicol.* **231**, 105740. (doi:10.1016/j.aquatox.2020.105740)

19. Kurihara H, Shirayama Y. 2004 Effects of increased atmospheric CO on sea urchin early development. *V ol.* **274**, 161–169.

20. Albright R, Langdon C. 2011 Ocean acidification impacts multiple early life history processes of the Caribbean coral Porites astreoides: OCEAN ACIDIFICATION IMPACTS CORAL RECRUITMENT. *Glob. Chang. Biol.* **17**, 2478–2487. (doi:10.1111/j.1365-2486.2011.02404.x)

21. Albright R, Mason B, Langdon C. 2008 Effect of aragonite saturation state on settlement and post-settlement growth of Porites astreoides larvae. *Coral Reefs* **27**, 485–490. (doi:10.1007/s00338-008-0392-5)

22. Moya A *et al.* 2012 Whole Transcriptome Analysis of the Coral *Acropora millepora* Reveals Complex Responses to CO_2-driven Acidification during the Initiation of Calcification. *Mol. Ecol.* **21**, 2440–2454. (doi:10.1111/j.1365-294X.2012.05554.x)

23. Nakamura M, Ohki S, Suzuki A, Sakai K. 2011 Coral larvae under ocean acidification: survival, metabolism, and metamorphosis. *PLoS One* **6**, e14521. (doi:10.1371/journal.pone.0014521)

24. Moya A, Huisman L, Forêt S, Gattuso J-P, Hayward DC, Ball EE, Miller DJ. 2015 Rapid acclimation of juvenile corals to CO_2-mediated acidification by upregulation of heat shock protein and Bcl-2 genes. *Mol. Ecol.* **24**, 438–452. (doi:10.1111/mec.13021)

25. Putnam HM, Mayfield AB, Fan TY, Chen CS, Gates RD. 2013 The physiological and molecular responses of larvae from the reef-building coral Pocillopora damicornis exposed to near-future increases in temperature and pCO2. *Mar. Biol.* **160**, 2157–2173. (doi:10.1007/s00227-012-2129-9)

26. Yuan X, Yuan T, Huang H, Jiang L, Zhou W, Liu S. 2018 Elevated CO2 delays the early development of scleractinian coral Acropora gemmifera. *Sci. Rep.* **8**, 2787. (doi:10.1038/s41598-018-21267-3)

27. Rivest EB, Hofmann GE. 2014 Responses of the metabolism of the larvae of Pocillopora damicornis to ocean acidification and warming. *PLoS One* **9**, e96172. (doi:10.1371/journal.pone.0096172)

28. Timmins-Schiffman E, O'Donnell MJ, Friedman CS, Roberts SB. 2013 Elevated pCO2 causes developmental delay in early larval Pacific oysters, Crassostrea gigas. *Marine Biology*. **160**, 1973–1982. (doi:10.1007/s00227-012-2055-x)

29. Foo SA, Dworjanyn SA, Poore AGB, Byrne M. 2012 Adaptive capacity of the habitat modifying sea urchin Centrostephanus rodgersii to ocean warming and ocean acidification: performance of early embryos. *PLoS One* **7**, e42497. (doi:10.1371/journal.pone.0042497)

30. Kelly MW, Padilla-Gamiño JL, Hofmann GE. 2013 Natural variation and the capacity to adapt to ocean acidification in the keystone sea urchin Strongylocentrotus purpuratus. *Glob. Chang. Biol.* **19**, 2536–2546. (doi:10.1111/gcb.12251)

31. O'Donnell MJ, Todgham AE, Sewell MA, Hammond LM, Ruggiero K, Fangue NA, Zippay ML, Hofmann GE. 2010 Ocean acidification alters skeletogenesis and gene expression in larval sea urchins. *Mar. Ecol. Prog. Ser.* **398**, 157–171.

32. Barton A, Hales B, Waldbusser GG, Langdon C, Feely RA. 2012 The Pacific oyster,Crassostrea gigas, shows negative correlation to naturally elevated carbon dioxide levels: Implications for near-term ocean acidification effects. *Limnol. Oceanogr.* **57**, 698–710. (doi:10.4319/lo.2012.57.3.0698)

33. Parker LM, Ross PM, O'connor WA. 2009 The effect of ocean acidification and temperature on the fertilization and embryonic development of the Sydney rock oysterSaccostrea glomerata(Gould 1850). *Glob. Chang. Biol.* **15**, 2123–2136. (doi:10.1111/j.1365-2486.2009.01895.x)

34. Parker LM, Ross PM, O'Connor WA. 2010 Comparing the effect of elevated pCO2 and temperature on the fertilization and early development of two species of oysters. *Marine Biology*. **157**, 2435–2452. (doi:10.1007/s00227-010-1508-3)

35. Barros P, Sobral P, Range P, Chícharo L, Matias D. 2013 Effects of sea-water acidification on fertilization and larval development of the oyster Crassostrea gigas. *J. Exp. Mar. Bio. Ecol.* **440**, 200–206. (doi:10.1016/j.jembe.2012.12.014)

36. Gazeau F, Gattuso J-P, Dawber C, Pronker AE, Peene F, Peene J, Heip CHR, Middelburg JJ. 2010 Effect of ocean acidification on the early life stages of the blue mussel Mytilus edulis. *Biogeosciences* **7**, 2051–2060. (doi:10.5194/bg-7-2051-2010)

37. Van Colen C, Debusschere E, Braeckman U, Van Gansbeke D, Vincx M. 2012 The early life history of the clam Macoma balthica in a high CO2 world. *PLoS One* **7**, e44655. (doi:10.1371/journal.pone.0044655)

38. Byrne M, Ho M, Selvakumaraswamy P, Nguyen HD, Dworjanyn SA, Davis AR. 2009 Temperature, but not pH, compromises sea urchin fertilization and early development under near-future climate change scenarios. *Proc. Biol. Sci.* **276**, 1883–1888. (doi:10.1098/rspb.2008.1935)

39. Ericson JA, Lamare MD, Morley SA, Barker MF. 2010 The response of two ecologically important Antarctic invertebrates (Sterechinus neumayeri and Parborlasia corrugatus) to reduced seawater pH: effects on fertilisation and embryonic development. *Mar. Biol.* **157**, 2689–2702. (doi:10.1007/s00227-010-1529-y)

40. Ericson JA, Ho MA, Miskelly A, King CK, Virtue P. 2012 Combined effects of two ocean change stressors, warming and acidification, on fertilization and early development of the Antarctic echinoid Sterechinus …. *Polar Biol.*

41. Dahlke FT, Lucassen M, Bickmeyer U, Wohlrab S, Puvanendran V, Mortensen A, Chierici M, Pörtner H-O, Storch D. 2020 Fish embryo vulnerability to combined acidification and warming coincides with a low capacity for homeostatic regulation. *J. Exp. Biol.* **223**. (doi:10.1242/jeb.212589)

42. Dahlke FT, Leo E, Mark FC, Pörtner H-O, Bickmeyer U, Frickenhaus S, Storch D. 2017 Effects of ocean acidification increase embryonic sensitivity to thermal extremes in Atlantic cod, Gadus morhua. *Glob. Chang. Biol.* **23**, 1499–1510. (doi:10.1111/gcb.13527)

43. Tadros W, Lipshitz HD. 2009 The maternal-to-zygotic transition: a play in two acts. *Development* **136**, 3033–3042. (doi:10.1242/dev.033183)

44. Vastenhouw NL, Cao WX, Lipshitz HD. 2019 The maternal-to-zygotic transition revisited. *Development* **146**. (doi:10.1242/dev.161471)

45. Chille EE, Strand E, Neder M, Schmidt V, Sherman M, Putnam HM, Mass T. 2021 Developmental series of gene expression clarifies maternal mRNA provisioning and maternal-to-zygotic transition in the reef-building coral Montipora capitata. *bioRxiv.* , 2021.04.14.439692. (doi:10.1101/2021.04.14.439692)

46. Van Etten J, Shumaker A, Mass T, Putnam HM, Bhattacharya D. 2020 Transcriptome analysis provides a blueprint of coral egg and sperm functions. *PeerJ*. **8**, e9739. (doi:10.7717/peerj.9739)

47. Strader ME, Aglyamova GV, Matz MV. 2018 Molecular characterization of larval development from fertilization to metamorphosis in a reef-building coral. *BMC Genomics* **19**, 17. (doi:10.1186/s12864-017-4392-0)

48. Reyes-Bermudez A, Villar-Briones A, Ramirez-Portilla C, Hidaka M, Mikheyev AS. 2016 Developmental Progression in the Coral Acropora digitifera Is Controlled by Differential Expression of Distinct Regulatory Gene Networks. *Genome Biol. Evol.* **8**, 851–870. (doi:10.1093/gbe/evw042)

49. Helm RR, Siebert S, Tulin S, Smith J, Dunn CW. 2013 Characterization of differential transcript abundance through time during Nematostella vectensis development. *BMC Genomics* **14**, 266. (doi:10.1186/1471-2164-14-266)

50. Padilla-Gamiño JL, Gates RD. 2012 Spawning dynamics in the Hawaiian reef-building coral Montipora capitata. *Mar. Ecol. Prog. Ser.* **449**, 145–160. (doi:10.3354/meps09530)

51. Heyward, AJ. 1986 Sexual reproduction in five species of the coral Montipora. *Hawaii Institute of Marine Biology, Technical Report* **37**, 170–178.

52. Shaw EC, Hamylton SM, Phinn SR. 2016 Incorporating benthic community changes into hydrochemical-based projections of coral reef calcium carbonate production under ocean acidification. *Coral Reefs*. **35**, 739–750. (doi:10.1007/s00338-016-1407-2)

53. Jury CP, Thomas FIM, Atkinson MJ, Toonen RJ. 2013 Buffer Capacity, Ecosystem Feedbacks, and Seawater Chemistry under Global Change. *Water* **5**, 1303–1325. (doi:10.3390/w5031303)

54. Drupp P, De Carlo EH, Mackenzie FT, Bienfang P, Sabine CL. 2011 Nutrient Inputs, Phytoplankton Response, and CO2 Variations in a Semi-Enclosed Subtropical Embayment, Kaneohe Bay, Hawaii. *Aquat. Geochem.* **17**, 473–498. (doi:10.1007/s10498-010-9115-y)

55. Gattuso J-P, Epitalon J-M, Lavigne H, Orr J, Gentili B, Hofmann A, Proye A, Soetaert K, Rae J. 2015 seacarb: Seawater carbonate chemistry. *R package version* **3**.

56. Perez FF, Fraga F. 1987 Association constant of fluoride and hydrogen ions in seawater. *Mar. Chem.* **21**, 161–168. (doi:10.1016/0304-4203(87)90036-3)

57. Lueker TJ, Dickson AG, Keeling CD. 2000 Ocean pCO2 calculated from dissolved inorganic carbon, alkalinity, and equations for K1 and K2: validation based on laboratory measurements of CO2 in gas and seawater at equilibrium. *Mar. Chem.* **70**, 105–119. (doi:10.1016/S0304-4203(00)00022-0)

58. Dickson AG. 1990 Standard potential of the reaction: AgCl(s) + 12H2(g) = Ag(s) + HCl(aq), and and the standard acidity constant of the ion HSO4− in synthetic sea water from 273.15 to 318.15 K. *J. Chem. Thermodyn.* **22**, 113–127. (doi:10.1016/0021-9614(90)90074-Z)

59. Dickson AG, Sabine CL, Christian JR. 2007 *Guide to best practices for ocean CO2 measurements*. North Pacific Marine Science Organization. See https://repository.oceanbestpractices.org/handle/11329/249.

60. RStudio Team. 2020 *RStudio: Integrated Development for R*. Boston, MA: RStudio, PBC. See http://www.rstudio.com/.

61. R Core Team. 2013 R: A language and environment for statistical computing.

62. Shumaker A *et al.* 2019 Genome analysis of the rice coral Montipora capitata. *Sci. Rep.* **9**, 2571. (doi:10.1038/s41598-019-39274-3)

63. Kim D, Paggi JM, Park C, Bennett C, Salzberg SL. 2019 Graph-based genome alignment and genotyping with HISAT2 and HISAT-genotype. *Nat. Biotechnol.* **37**, 907–915. (doi:10.1038/s41587-019-0201-4)

64. Pertea M, Pertea GM, Antonescu CM, Chang T-C, Mendell JT, Salzberg SL. 2015 StringTie enables improved reconstruction of a transcriptome from RNA-seq reads. *Nat. Biotechnol.* **33**, 290–295. (doi:10.1038/nbt.3122)

65. Gentleman R, Carey V, Huber W, Hahne F. 2020 *genefilter: genefilter: methods for filtering genes from high-throughput experiments*.

66. Love M, Huber W, Anders S. 2014 Moderated estimation of fold change and dispersion for RNA-seq data with DESeq2. *Genome Biol.* **15**, 550. (doi:10.1186/s13059-014-0550-8)

67. Love M, Anders S, Huber W. 2014 Differential analysis of count data--the DESeq2 package. *Genome Biol.* **15**, 10–1186.

68. Chen H, Boutros PC. 2011 VennDiagram: a package for the generation of highly-customizable Venn and Euler diagrams in R. *BMC Bioinformatics* **12**, 35. (doi:10.1186/1471-2105-12-35)

69. Gu Z, Eils R, Schlesner M. 2016 Complex heatmaps reveal patterns and correlations in multidimensional genomic data. *Bioinformatics* **32**, 2847–2849. (doi:10.1093/bioinformatics/btw313)

70. Malika C, Ghazzali N, Boiteau V, Niknafs A. 2014 NbClust: an R package for determining the relevant number of clusters in a data Set. *J. Stat. Softw.* **61**, 1–36.

71. Young MD, Wakefield MJ, Smyth GK, Oshlack A. 2010 Gene ontology analysis for RNA-seq: accounting for selection bias. *Genome Biol.* **11**, R14. (doi:10.1186/gb-2010-11-2-r14)

72. Ashburner M *et al.* 2000 Gene ontology: tool for the unification of biology. The Gene Ontology Consortium. *Nat. Genet.* **25**, 25–29. (doi:10.1038/75556)

73. Wickham H. 2011 ggplot2: ggplot2. *Wiley Interdiscip. Rev. Comput. Stat.* **3**, 180–185. (doi:10.1002/wics.147)

74. Grabherr MG *et al.* 2011 Full-length transcriptome assembly from RNA-Seq data without a reference genome. *Nat. Biotechnol.* **29**, 644–652. (doi:10.1038/nbt.1883)

75. Simão FA, Waterhouse RM, Ioannidis P, Kriventseva EV, Zdobnov EM. 2015 BUSCO: assessing genome assembly and annotation completeness with single-copy orthologs. *Bioinformatics* **31**, 3210–3212. (doi:10.1093/bioinformatics/btv351)

76. Voolstra C *et al.* 2015 The ReFuGe 2020 Consortium—using 'omics' approaches to explore the adaptability and resilience of coral holobionts to environmental change. *Frontiers in Marine Science* **2**, 68. (doi:10.3389/fmars.2015.00068)

77. Liew YJ, Aranda M, Voolstra CR. 2016 Reefgenomics.Org - a repository for marine genomics data. *Database.* **2016**, baw152. (doi:10.1093/database/baw152)

78. Li B, Dewey CN. 2011 RSEM: accurate transcript quantification from RNA-Seq data with or without a reference genome. *BMC Bioinformatics* **12**, 323. (doi:10.1186/1471-2105-12-323)

79. Langmead B. 2010 Aligning short sequencing reads with Bowtie. *Curr. Protoc. Bioinformatics* **Chapter 11**, Unit 11.7. (doi:10.1002/0471250953.bi1107s32)

80. Altschul SF, Madden TL, Schäffer AA, Zhang J, Zhang Z, Miller W, Lipman DJ. 1997 Gapped BLAST and PSI-BLAST: a new generation of protein database search programs. *Nucleic Acids Res.* **25**, 3389–3402. (doi:10.1093/nar/25.17.3389)

81. Chua CM, Leggat W, Moya A, Baird AH. 2013 Temperature affects the early life history stages of corals more than near future ocean acidification. *Mar. Ecol. Prog. Ser.* **475**, 85–92. (doi:10.3354/meps10077)

82. Chua CM, Leggat W, Moya A, Baird AH. 2013 Near-future reductions in pH will have no consistent ecological effects on the early life-history stages of reef corals. *Mar. Ecol. Prog. Ser.* **486**, 143–151. (doi:10.3354/meps10318)

83. Hamdoun A, Epel D. 2007 Embryo stability and vulnerability in an always changing world. *Proc. Natl. Acad. Sci. U. S. A.* **104**, 1745–1750. (doi:10.1073/pnas.0610108104)

84. Ries JB. 2011 A physicochemical framework for interpreting the biological calcification response to CO2-induced ocean acidification. *Geochim. Cosmochim. Acta* **75**, 4053–4064. (doi:10.1016/j.gca.2011.04.025)

85. Akiva A, Neder M, Kahil K, Gavriel R, Pinkas I, Goobes G, Mass T. 2018 Minerals in the pre-settled coral Stylophora pistillata crystallize via protein and ion changes. *Nat. Commun.* **9**, 1880. (doi:10.1038/s41467-018-04285-7)

86. Mass T, Putnam HM, Drake JL, Zelzion E, Gates RD, Bhattacharya D, Falkowski PG. 2016 Temporal and spatial expression patterns of biomineralization proteins during early development in the stony coral Pocillopora damicornis. *Proceedings of the Royal Society B: Biological Sciences* **283**. (doi:10.1098/rspb.2016.0322)

87. DeCarlo TM, Comeau S, Cornwall CE, McCulloch MT. 2018 Coral resistance to ocean acidification linked to increased calcium at the site of calcification. *Proc. Biol. Sci.* **285**. (doi:10.1098/rspb.2018.0564)

88. Comeau S, Cornwall CE, DeCarlo TM, Krieger E, McCulloch MT. 2018 Similar controls on calcification under ocean acidification across unrelated coral reef taxa. *Glob. Chang. Biol.* **24**, 4857–4868. (doi:10.1111/gcb.14379)

89. Zhao X, Han Y, Chen B, Xia B, Qu K, Liu G. 2020 CO2-driven ocean acidification weakens mussel shell defense capacity and induces global molecular compensatory responses. *Chemosphere* **243**, 125415. (doi:10.1016/j.chemosphere.2019.125415)

90. Davies SW, Marchetti A, Ries JB, Castillo KD. 2016 Thermal and pCO2 Stress Elicit Divergent Transcriptomic Responses in a Resilient Coral. *Frontiers in Marine Science* **3**, 112. (doi:10.3389/fmars.2016.00112)

91. Vidal-Dupiol J *et al.* 2013 Genes related to ion-transport and energy production are upregulated in response to CO2-driven pH decrease in corals: new insights from transcriptome analysis. *PLoS One* **8**, e58652. (doi:10.1371/journal.pone.0058652)

92. Alamaru A, Yam R, Shemesh A, Loya Y. 2009 Trophic biology of Stylophora pistillata larvae: evidence from stable isotope analysis. *Mar. Ecol. Prog. Ser.* **383**, 85–94. (doi:10.3354/meps07958)

93. Ben-David-Zaslow R, Benayahu Y. 2000 Biochemical composition, metabolism, and amino acid transport in planula-larvae of the soft coral Heteroxenia fuscescens. *J. Exp.*

Zool. **287**, 401–412. (doi:10.1002/1097-010x(20001101)287:6<401::aid-jez1>3.0.co;2-4)

94. Harii S, Yamamoto M, Hoegh-Guldberg O. 2010 The relative contribution of dinoflagellate photosynthesis and stored lipids to the survivorship of symbiotic larvae of the reef-building corals. *Mar. Biol.* **157**, 1215–1224. (doi:10.1007/s00227-010-1401-0)

95. Reipschläger A, Pörtner HO. 1996 Metabolic depression during environmental stress: the role of extracellular versus intracellular pH in Sipunculus nudus. *J. Exp. Biol.* **199**, 1801–1807.

96. Kaniewska P, Campbell PR, Kline DI, Rodriguez-Lanetty M, Miller DJ, Dove S, Hoegh-Guldberg O. 2012 Major cellular and physiological impacts of ocean acidification on a reef building coral. *PLoS One* **7**, e34659. (doi:10.1371/journal.pone.0034659)

97. Björklund M. 2019 Cell size homeostasis: Metabolic control of growth and cell division. *Biochim. Biophys. Acta Mol. Cell Res.* **1866**, 409–417. (doi:10.1016/j.bbamcr.2018.10.002)

98. Miettinen TP, Björklund M. 2017 Mitochondrial Function and Cell Size: An Allometric Relationship. *Trends Cell Biol.* **27**, 393–402. (doi:10.1016/j.tcb.2017.02.006)

99. Liew YJ *et al.* 2018 Epigenome-associated phenotypic acclimatization to ocean acidification in a reef-building coral. *Sci Adv* **4**, eaar8028. (doi:10.1126/sciadv.aar8028)

100. Tominaga T, Barber DL. 1998 Na–H Exchange Acts Downstream of RhoA to Regulate Integrin-induced Cell Adhesion and Spreading. *MBoC* **9**, 2287–2303. (doi:10.1091/mbc.9.8.2287)

101. Fernandes PN, Mannarino SC, Silva CG, Pereira MD, Panek AD, Eleutherio ECA. 2007 Oxidative stress response in eukaryotes: effect of glutathione, superoxide dismutase and catalase on adaptation to peroxide and menadione stresses inSaccharomyces cerevisiae. *Redox Report*. **12**, 236–244. (doi:10.1179/135100007x200344)

102. Martínez R. 2007 Effects of ultraviolet radiation on protein content, respiratory electron transport system (ETS) activity and superoxide dismutase (SOD) activity of Antarctic plankton. *Polar Biol.* **30**, 1159–1172. (doi:10.1007/s00300-007-0273-3)

103. Zhao X, Ren X, Zhu R, Luo Z, Ren B. 2016 Zinc oxide nanoparticles induce oxidative DNA damage and ROS-triggered mitochondria-mediated apoptosis in zebrafish embryos. *Aquat. Toxicol.* **180**, 56–70. (doi:10.1016/j.aquatox.2016.09.013)

104. Sampayo JN, Olsen A, Lithgow GJ. 2003 Oxidative stress in Caenorhabditis elegans: protective effects of superoxide dismutase/catalase mimetics. *Aging Cell* **2**, 319–326. (doi:10.1046/j.1474-9728.2003.00063.x)

105. DeSalvo MK, Voolstra CR, Sunagawa S, Schwarz JA, Stillman JH, Coffroth MA, Szmant AM, Medina M. 2008 Differential gene expression during thermal stress and bleaching in the Caribbean coral Montastraea faveolata. *Mol. Ecol.* **17**, 3952–3971. (doi:10.1111/j.1365-294X.2008.03879.x)

106. Lesser MP, Farrell JH. 2004 Exposure to solar radiation increases damage to both host tissues and algal symbionts of corals during thermal stress. *Coral Reefs* **23**, 367–377. (doi:10.1007/s00338-004-0392-z)

107. DeSalvo MK, Sunagawa S, Voolstra CR, Medina M. 2010 Transcriptomic responses to heat stress and bleaching in the elkhorn coral Acropora palmata. *Mar. Ecol. Prog. Ser.* **402**, 97–113. (doi:10.3354/meps08372)

108. van de Water JAJM, Ainsworth TD, Leggat W, Bourne DG, Willis BL, van Oppen MJH. 2015 The coral immune response facilitates protection against microbes during tissue regeneration. *Mol. Ecol.* **24**, 3390–3404. (doi:10.1111/mec.13257)

109. Fuchs Y, Steller H. 2015 Live to die another way: modes of programmed cell death and the signals emanating from dying cells. *Nat. Rev. Mol. Cell Biol.* **16**, 329–344. (doi:10.1038/nrm3999)

110. Linkermann A, Green DR. 2014 Necroptosis. *N. Engl. J. Med.* **370**, 455–465. (doi:10.1056/NEJMra1310050)

111. Todgham AE, Hofmann GE. 2009 Transcriptomic response of sea urchin larvae Strongylocentrotus purpuratus to CO2-driven seawater acidification. *J. Exp. Biol.* **212**, 2579–2594. (doi:10.1242/jeb.032540)

112. Poquita-Du RC, Huang D, Chou LM, Mrinalini, Todd PA. 2019 Short Term Exposure to Heat and Sediment Triggers Changes in Coral Gene Expression and Photo-Physiological Performance. *Frontiers in Marine Science*. **6**. (doi:10.3389/fmars.2019.00121)

113. Rosic N, Kaniewska P, Chan C-KK, Ling EYS, Edwards D, Dove S, Hoegh-Guldberg O. 2014 Early transcriptional changes in the reef-building coral Acropora aspera in response to thermal and nutrient stress. *BMC Genomics* **15**, 1052. (doi:10.1186/1471-2164-15-1052)

114. Polato NR, Altman NS, Baums IB. 2013 Variation in the transcriptional response of threatened coral larvae to elevated temperatures. *Mol. Ecol.* **22**, 1366–1382. (doi:10.1111/mec.12163)

115. Sokolova IM, Frederich M, Bagwe R, Lannig G, Sukhotin AA. 2012 Energy homeostasis as an integrative tool for assessing limits of environmental stress

tolerance in aquatic invertebrates. *Mar. Environ. Res.* **79**, 1–15. (doi:10.1016/j.marenvres.2012.04.003)

116. Reynaud S, Leclercq N, Romaine-Lioud S, Ferrier-Pagés C, Jaubert J, Gattuso J-P. 2003 Interacting effects of CO2 partial pressure and temperature on photosynthesis and calcification in a scleractinian coral: EFFECTS OF p CO2 AND TEMPERATURE ON CORAL. *Glob. Chang. Biol.* **9**, 1660–1668. (doi:10.1046/j.1365-2486.2003.00678.x)

117. Krief S, Hendy EJ, Fine M, Yam R, Meibom A, Foster GL, Shemesh A. 2010 Physiological and isotopic responses of scleractinian corals to ocean acidification. *Geochim. Cosmochim. Acta* **74**, 4988–5001. (doi:10.1016/j.gca.2010.05.023)

118. Guillermic M *et al.* 2021 Thermal stress reduces pocilloporid coral resilience to ocean acidification by impairing control over calcifying fluid chemistry. *Sci Adv* **7**. (doi:10.1126/sciadv.aba9958)

119. Scucchia F, Malik A, Zaslansky P, Putnam HM, Mass T. 2021 Combined responses of primary coral polyps and their algal endosymbionts to decreasing seawater pH.

120. Gibbin EM, Putnam HM, Davy SK, Gates RD. 2014 Intracellular pH and its response to CO2-driven seawater acidification in symbiotic versus non-symbiotic coral cells. *J. Exp. Biol.* **217**, 1963–1969. (doi:10.1242/jeb.099549)

121. Edmunds PJ, Cumbo VR, Fan T-Y. 2013 Metabolic costs of larval settlement and metamorphosis in the coral Seriatopora caliendrum under ambient and elevated pCO2. *J. Exp. Mar. Bio. Ecol.* **443**, 33–38. (doi:10.1016/j.jembe.2013.02.032)

122. Hughes TP, Tanner JE. 2000 Recruitment failure, life histories, and long-term decline of Caribbean corals. *Ecology* **81**, 2250–2263.

123. Putnam HM. 2021 Avenues of reef-building coral acclimatization in response to rapid environmental change. *J. Exp. Biol.* **224**. (doi:10.1242/jeb.239319)

Tables and Figures

Table 1. Descriptive statistics for temperature, salinity, and carbonate chemistry across the 9 days of exposure (mean ± standard error of the mean).

	n	Temp (°C)	Sal (psu)	pH (Total Scale)	TA (µmol kg^{-1})	pCO_2 (µmol kg^{-1})	CO_3^{-2} (µmol kg^{-1})	HCO_3 (µmol kg^{-1})	DIC (µmol kg^{-1})	Aragonite Saturation State
pH 7.8 (Amb)	50	26.67±0.08	34.27±0.02	7.848±0.006	2210.5±5	661.6±12.3	147.5±1.8	1847.4±6.7	2012.8±5.8	2.37±0.03
pH 7.6 (Low)	48	26.61±0.09	34.29±0.02	7.607±0.007	2210.9±9	1238.2±22.6	91.0±1.1	1987.2±8.5	2111.9±8.8	1.46±0.02
pH 7.3 (Xlow)	46	26.65±0.08	34.25±0.02	7.324±0.007	2205.4±3	2491.2±47.3	49.8±0.7	2083.2±3.8	2200.8±4.3	0.80±0.01

Figure 1. Summary of A) experimental design and B) sampling timeline, including example photographs of each life stage. Early life stages were exposed to treatment immediately after fertilization. Size analyses were performed on all life stages starting with Unfertilized Eggs (0 hpf). Gene expression analyses were performed on the samples following fertilization corresponding to fertilized eggs (1 hpf), cleavage (4 hpf), prawn chip (9 hpf), early gastrula (14 hpf) and swimming larvae (planula, 9 dpf).

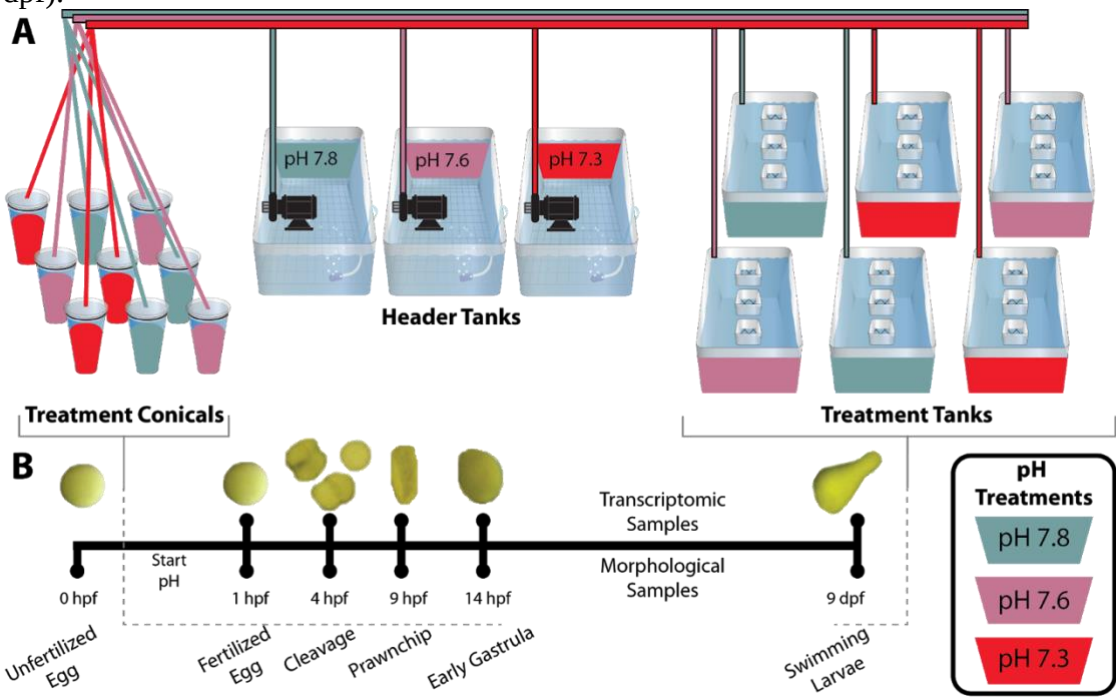

Figure 2. Developmental age and size. a) Proportion of embryos at each cleavage stage at 4 HPF and volume (mm^3) of b) unfertilized eggs, c) fertilized eggs, d) early gastrula, and e) planula in each treatment. Prawn chip stages were not analyzed given the fold in the morphology which generates added assumptions for volume calculations (See Fig. 1B prawn chip picture).

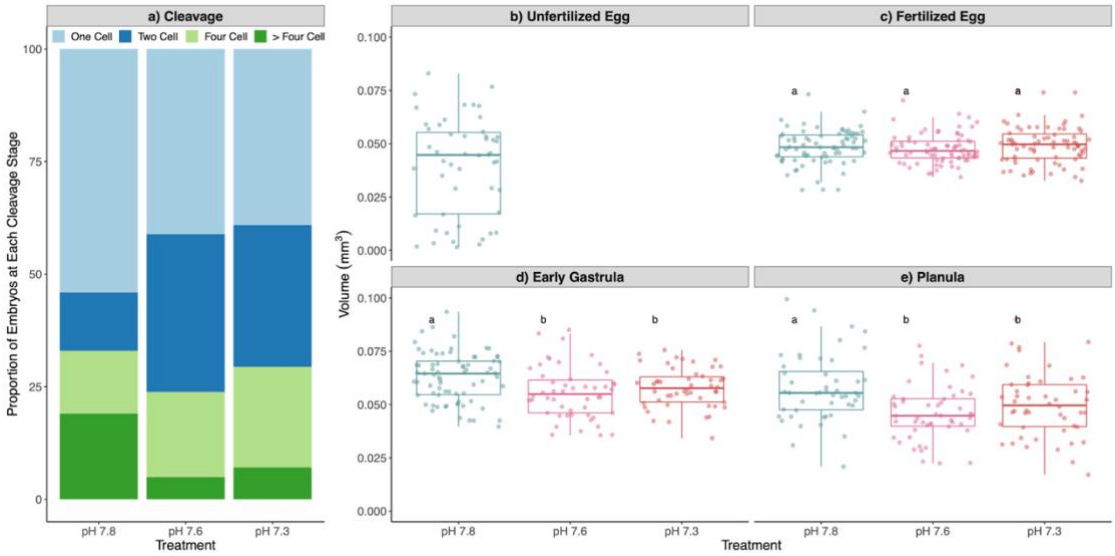

Figure 3. a) Principal coordinates analysis of all life stages based on sample-to-sample distance computed from all genes passing a low counts filter, wherein a gene must have a count of 10 or greater in at least 2 out of the 41 samples (pOverA ~0.05, 10). b) shows principal coordinates analysis of the sample-to-sample distance of planula samples, only (pOverA ~0.875, 10).

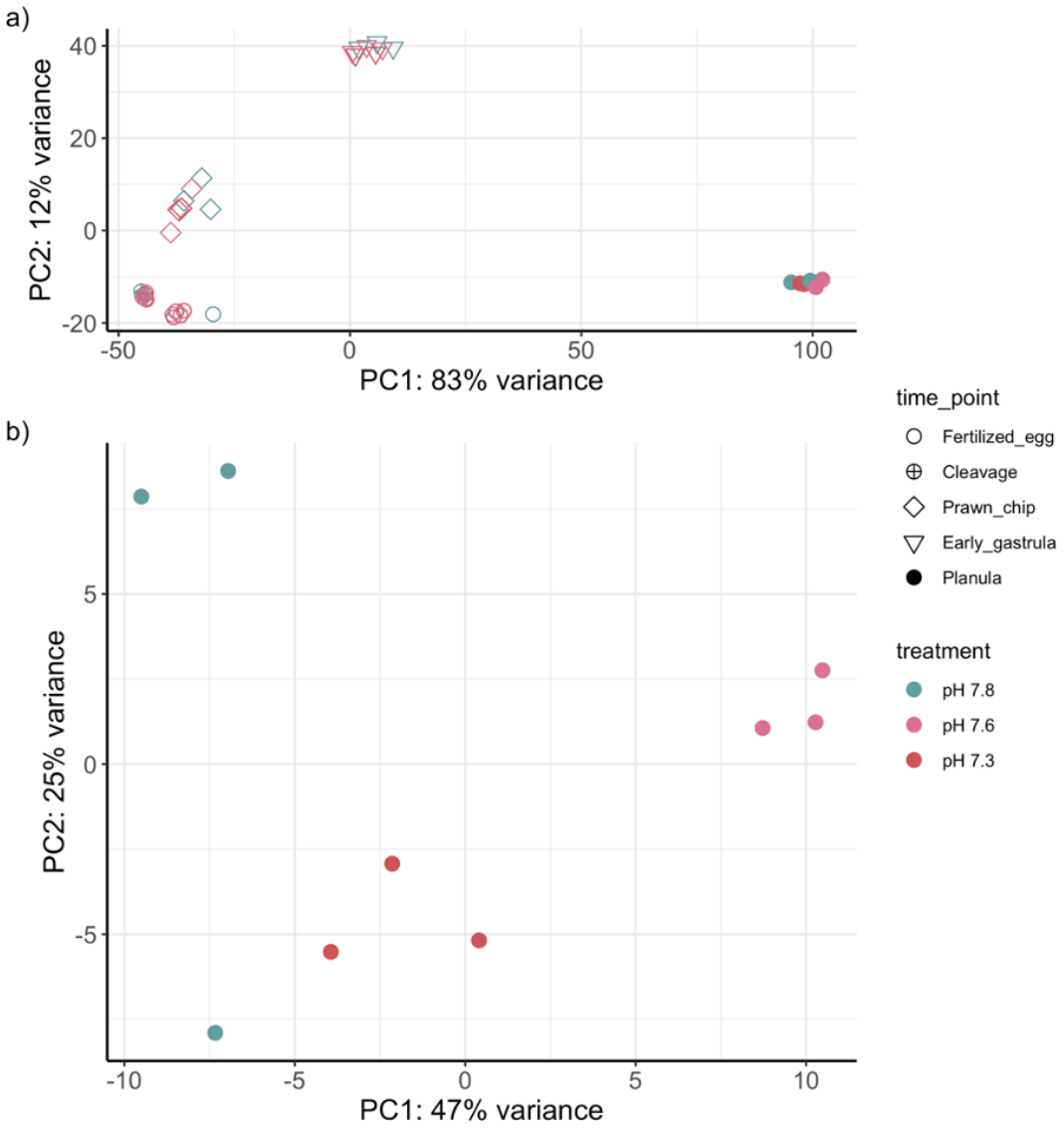

Figure 4. a) Venn diagram and b) heatmap of all genes that are differentially-expressed between treatments at the planula stage. Clusters in the heatmap are based on k-means clustering using the R program NBclust to calculate the optimal number of clusters using 30 indices. Heatmap colors for each gene are based on difference in expression compared to average VST across all samples, where red cells are more highly expressed compared to the rowmean and blue cells more lowly expressed compared to the rowmean.

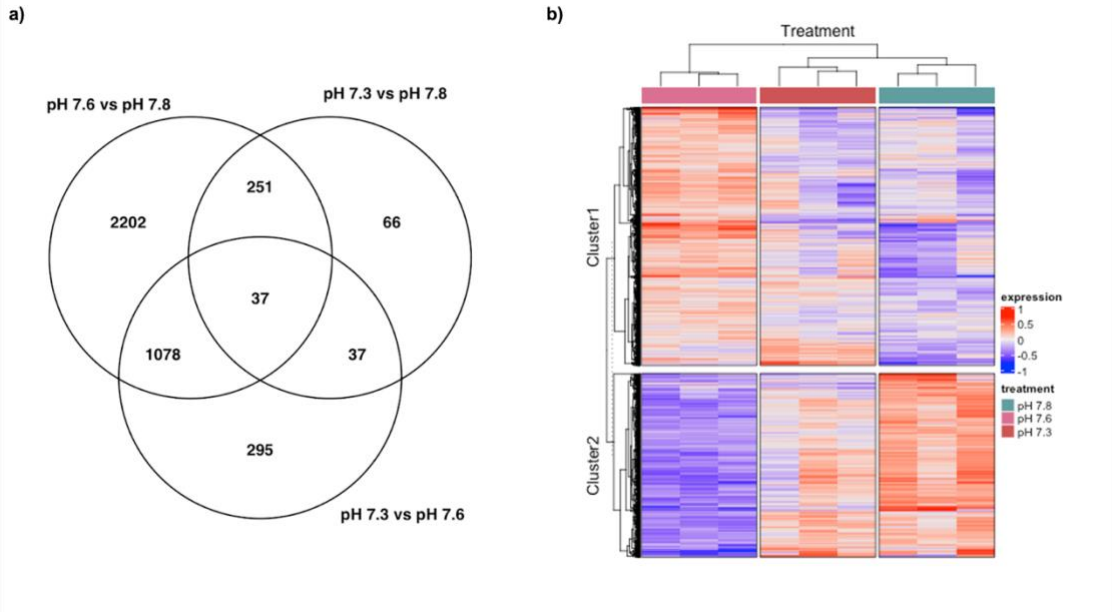

Figure 5. a) Biological process and b) Molecular Function terms that are enriched in planula developing in the low treatment compared to the extreme low and ambient treatments. Up = Terms associated with DEGs (p-adjusted<0.05, log2FoldChange>1, numInCat>5) from Cluster 1, Down = terms associated with DEGs (p-adjusted<0.05, log2FoldChange>1, numInCat>5) from Cluster 2.

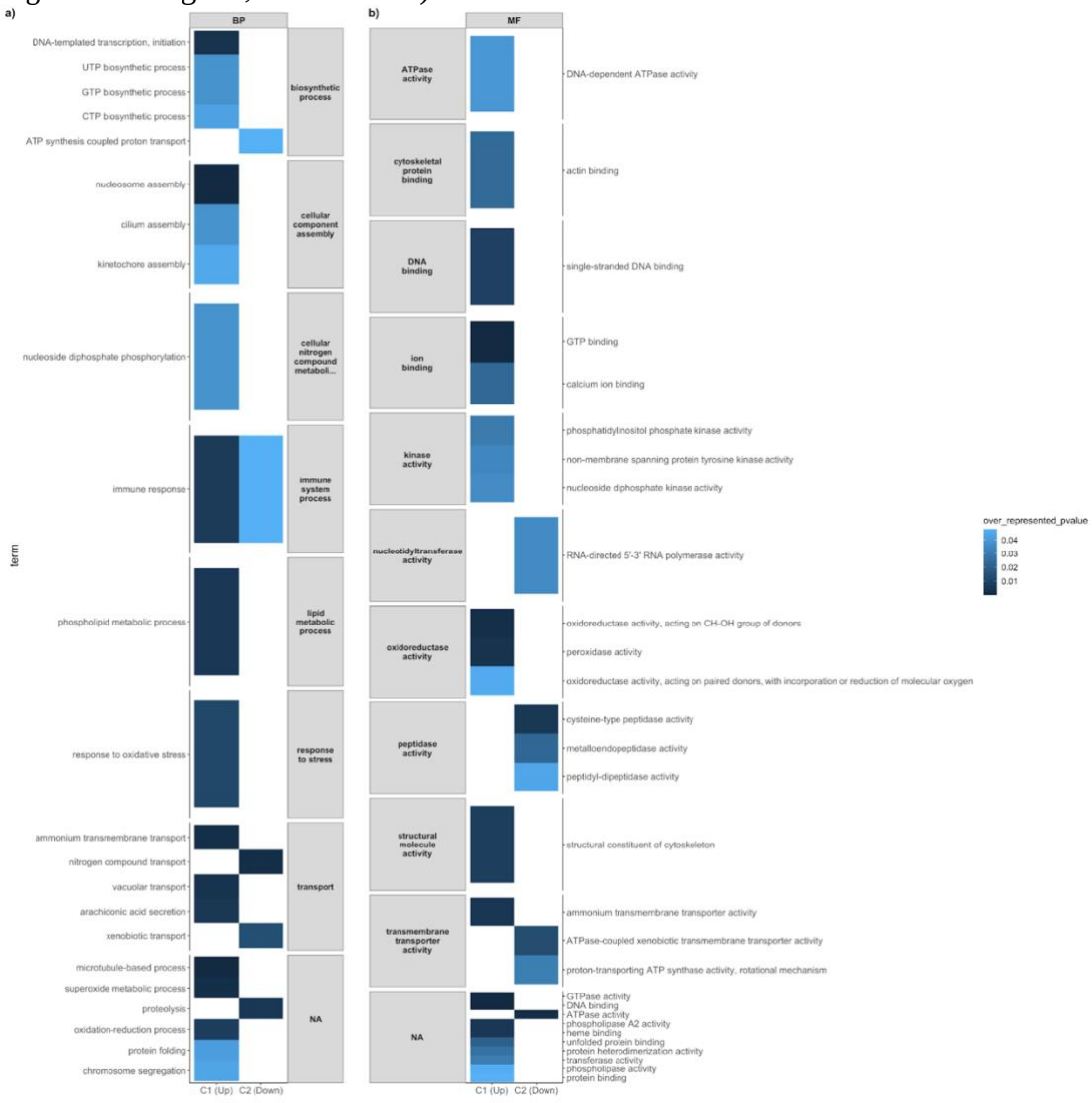

.

APPENDICES

Supplementary Material for Manuscript 1

Developmental series of gene expression clarifies maternal mRNA provisioning and maternal-to-zygotic transition in the reef-building coral *Montipora capitata*"

Chille E, Strand E, Neder M, Schmidt V, Sherman M, Mass T, Putnam HM

Figure S1. Boxplot and overlaid points of mean eigengene expression value of each of the replicate samples per time point (n=3, except mid-gastrula and late-gastrula where n=2) for each WGCNA module cluster (A-I).

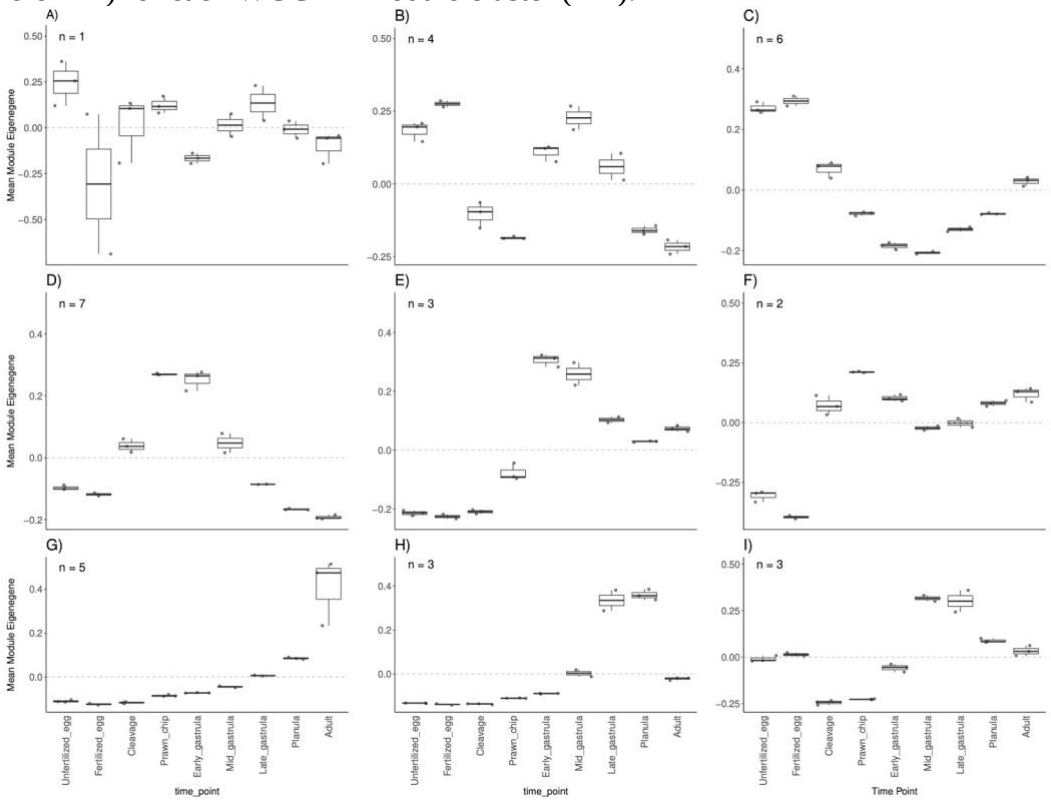

Table S1. Results from functional annotation of the genome using DIAMOND, InterProScan, Blast2GO, and Uniprot: 200824_Mcap_Blast_GO_KO.tsv

Table S2. Significant biological process, molecular function, and cellular component gene ontology terms for each life stage. Results are sorted by time point and then by p-value of over-represented terms: GO.05.allDev.csv

Table S3. Significant biology process and molecular function gene ontology terms for the maternal mRNA complement. Results are sorted by time point, ontology, and p-value of over-represented terms: GO.05.Mat.csv

Table S4. Significant biology process and molecular function gene ontology terms for the first wave of the MZT. Results are sorted by time point, ontology, and p-value of over-represented terms: GO.05.ZGA1.csv

Table S5. Significant biology process and molecular function gene ontology terms for the second wave of the MZT. Results are sorted by time point, ontology, and p-value of over-represented terms: GO.05.ZGA2.csv

Table S6. Significant biology process and molecular function gene ontology terms for the second wave of the adult. Results are sorted by time point, ontology, and p-value of over-represented terms: GO.05.Adult.csv

Table S7. Differential expression analysis results from the 12 biomarkers genes (Figures 6 (A) and 7 (B)) with significant (padj<0.05, log2FoldChange>|1|) up- and down-regulation. Results are sorted by order by Figure 6 (A) and 7 (B), followed by life stage: all_biomarker_DEGs.csv

Table S8. Top 10 hits to developmental biomarkers (A) and methylation-related enzymes (B) in the *M. capitata* transcriptome. Results are sorted by order in Figures 6 (A) and 7 (B) followed by bitscore. Only the first entry for each enzyme was plotted to examine expression profiles: Epi_MTZ_biomarker_hits_Top10.csv

Supplementary Material for Manuscript 2

Development in corals with vertically transmitted symbionts is resistant to ocean acidification

Chille E, Strand E, Scucchia F, Neder M, Schmidt V, Sherman M, Mass T, Putnam HM

Table S1 - Discrete measurements for temperature, salinity, and OA chemistry corresponding to Table 1: Seawater_chemistry_table_Output_All.csv

Figure S1 - Principal coordinates analysis of A) fertilized eggs, B) cleaving embryos, C) prawn chip, and D) early gastrula based on sample-to-sample distance computed from genes passing a low counts filter, wherein a gene must have a count of 10 or greater in at least 7 out of 8 samples (pOverA ~0.875, 10).

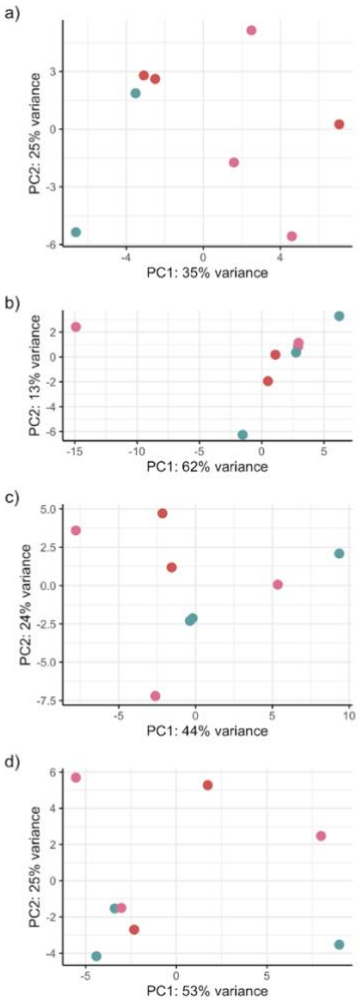

Table S2 - Differential gene expression and k-means clustering (k=2) results for planula: pln_DEGs_all.csv

Table S3 - GOseq enrichment summary statistics with GOslim data and identifiers of associated differentially-expressed genes: GOenrichmentsummary.csv

Figure S2 - Principal coordinates analysis of symbiont genes in the planula samples. a) A principal coordinates analysis based on sample-to-sample distance computed from the 1,365 genes passing a low counts filter, wherein a gene must have a count of 10 or greater in at least 7 out of 8 samples (pOverA ~0.875, 10). b) A principal coordinates analysis based on sample-to-sample distance computed from the 29 symbiont genes differentially expressed in planula developing in different pH environments.

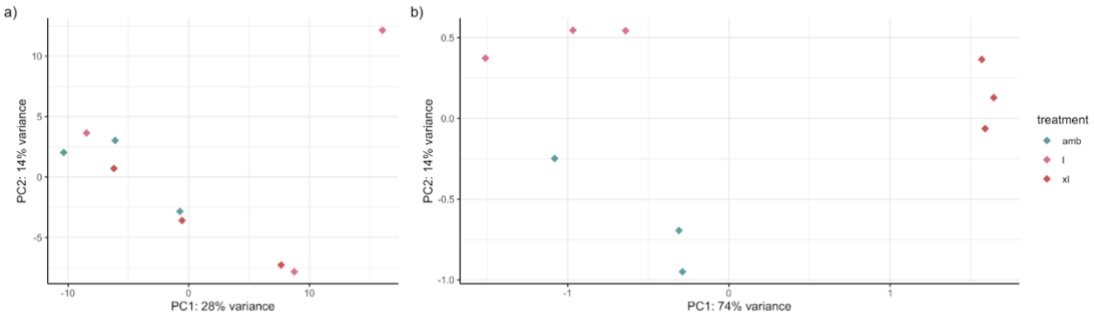

Table S4 - Differential gene expression of symbionts extracted from planula holobiont mRNA samples: symDEG_results.csv

Table S5 - Blastx alignment summary of the 29 differentially-expressed symbiont genes in the planula holobiont samples to the NCBI non-redundant database: symDEG_blast_summary.csv